HAL
open science

# A new conceptual methodology for interpretation of mass transport processes from seismic data

Pauline Le Bouteiller, Sara Lafuerza, Jean Charlety, Antonio Tadeu Reis, Didier Granjeon, Florence Delprat-Jannaud, Christian Gorini

## To cite this version:

Pauline Le Bouteiller, Sara Lafuerza, Jean Charlety, Antonio Tadeu Reis, Didier Granjeon, et al.. A new conceptual methodology for interpretation of mass transport processes from seismic data. Marine and Petroleum Geology, 2019, 103, pp.438-455. 10.1016/j.marpetgeo.2018.12.027 . hal-02117343

**HAL Id: hal-02117343**

**https://ifp.hal.science/hal-02117343**

Submitted on 2 May 2019

**HAL** is a multi-disciplinary open access archive for the deposit and dissemination of scientific research documents, whether they are published or not. The documents may come from teaching and research institutions in France or abroad, or from public or private research centers.

L'archive ouverte pluridisciplinaire **HAL**, est destinée au dépôt et à la diffusion de documents scientifiques de niveau recherche, publiés ou non, émanant des établissements d'enseignement et de recherche français ou étrangers, des laboratoires publics ou privés.

ACCEPTED MANUSCRIPT

# A new conceptual methodology for interpretation of mass transport processes from seismic data

Corresponding author: Pauline Le Bouteiller[a, b,1]: pauline.le_bouteiller@upmc.fr
Sara Lafuerza[b]: sara.lafuerza@upmc.fr
Jean Charléty[a]: jean.charlety@ifpen.fr
Antonio Tadeu Reis[c]: antonio.tadeu@pq.cnpq.br
Didier Granjeon[a]: didier.granjeon@ifpen.fr
Florence Delprat-Jannaud[a]: florence.delprat-jannaud@ifpen.fr
Christian Gorini[b]: christian.gorini@upmc.fr

[a] : IFP Energies nouvelles; 1 avenue du Bois-Préau, F-92852 Rueil-Malmaison, France.
[b] : Sorbonne Université, CNRS-INSU, Institut des Sciences de la Terre de Paris, ISTeP UMR 719; 1 place Jussieu, F-75005 Paris, France
[c] : School of Oceanography/FAOC, Universidade do Estado do Rio de Janeiro (UERJ); Rua São Francisco Xavier, 524, 4° andar, Bloco E; Maracaña, Rio de Janeiro, RJ, CEP 20550-900, Brazil.

## Highlights

- MTD interpretation is enhanced by a standardized graph-based methodology
- The proposed methodology integrates the variability of MTD physical processes
- The methodology is to be shared and improved by the interpretation community

## Abstract

Identification and seismic mapping of mass-transport deposits (MTDs) are vital targets for marine geological studies both for a better understanding of mass wasting processes and geohazards and for economic prospects in sedimentary basins. In recent decades, refinements in the interpretation of these geobodies have benefited from increasingly good quality 3D seismic data. However, approaches to define the characteristics, rheology and mechanics of such slope failure deposits still rely mainly on inferences from case-dependent interpretations of these stratigraphic elements; what is more, features and seismic characteristics of MTDs may vary significantly from one case to another, implying the existence of many different environments and related physics. This makes the study of submarine mass movement a challenging task for a seismic interpreter. In this paper, we present a new conceptual analytical method based on an objective approach for interpreting the wide range of diverse objects related to mass wasting, in order to minimize seismic interpretation subjectivity. We propose an ontology-like methodology, based on a conceptual organization of a diversity of interpretation elements arranged in a knowledge base. MTDs are considered as objects

[1] Permanent address : pauline.lebouteiller@mines-paris.org

with representative properties, each one characterized by several descriptors, which are themselves impacted by multiple physical processes in a graph-based conception. We thus propose a method to infer the most probable interpretations for one mass movement from its deposit characteristics. We applied our graph-based methodology to two MTDs delineated in 3D seismic data in the Offshore Amazon Basin, Brazil. Based on the analysis of all MTD properties and their possible causes, several candidate interpretations were provided. The~~se~~ interpretations yielded by the graph are in line with the known geology and instability processes of the region, thereby validating the feasibility of the approach. The next development stage is a numerical definition of the knowledge base for further sharing and operability.

**Keywords**

Mass transport deposits

Mass transport processes

Submarine slope failures

Seismic interpretation

Knowledge-based interpretation

Ontology

ACCEPTED MANUSCRIPT

# 1. Introduction

Mass transport deposits (MTDs) are geological bodies resulting from gravity-driven downslope mass movement. As such, they are an invaluable source of information on instability events themselves, and yield insights for current assessment of continental slope geohazards. Submarine slope failures have been shown to contribute significantly to sediment transport and sedimentary records in some basins (e.g. Lee *et al.*, 2007, Shipp *et al.*, 2011). Research on their genesis and evolution should improve stratigraphic analyses on basin infilling and geometries; it may also provide information on their economic petroleum potential and industrial hazard assessment (Alves, 2015).

The literature reports that MTD objects can provide direct information on former processes in a basin. Existing classifications of MTDs (e.g., Varnes, 1958; Mulder & Alexander, 2001b; Moscardelli & Wood, 2008; Posamentier & Martinsen, 2011; Talling *et al.*, 2012) illustrate this point correctly, as they tend to relate typical aspects of objects with typical failure-related processes. Classifications are usually based on a combination of internal and external features of the MTD, its depositional environment and the former event itself. Yet case-study interpretations are often site-specific and MTD objects do not always fit in widely validated classification schemes (Vanneste *et al.*, 2014). Similarly, large scale statistics on MTDs (e.g. Owen *et al.*, 2007, Leynaud *et al.*, 2009, Urgeles & Camerlenghi, 2013), although demonstrating links between MTD characteristics and different environments, may not always be applicable in different geological settings. However, a lot of knowledge is unquestionably already available on how to interpret features of MTD objects. The question we tackle here is how to interpret MTD history from their seismic signatures, using available knowledge as objectively as possible.

## 1.1. MTD characterization

Given the great complexity and variety of MTDs, their characterization may be a challenging task. In any case, MTD characterization from seismic data starts by a description of the geobody concerned. In such a description, it is important: (1) to include all relevant descriptive features; and (2) to use the information contained in the seismic data as much as possible. The wide variety of these features has been highlighted in the literature. They include: (i) geomorphologic features (e.g. Moscardelli & Wood, 2008), such as general shape and deposit geometry, spatial arrangement/continuity, recognizable 'tongues' showing deposit irregular extension, and a potentially visible headscarp, making it possible to relate MTDs to their original stratigraphic position and loci if not already known (e.g. Vanneste *et al.*, 2014); (ii) kinematic indicators (Bull *et al.*, 2009), such as evidence for flow direction, deformation and/or erosional markers and signs of compression/extension; (iii)

stratigraphic elements, such as their position in the depositional succession for timing precision and any attempt to date the deposit. Internal features of MTDs are also valuable to infer event-related processes. Yet the internal architecture of MTDs, and their lateral facies variability, are not often taken into account (e.g. Ortiz-Karpf *et al.*, 2016). 3D seismic data may provide useful information in this respect (e.g. Frey-Martínez, 2010). Thanks to their higher resolution and two horizontal directions, 3D data enable refined and more reliable quantitative characterization of the properties of the object, although extra working time may be required for analysis compared with studies using 2D data. Spatial distribution of several MTDs in a basin also proves useful to assess the frequency of slope failure (e.g. Urgeles & Camerlenghi, 2013), as well as the evolution of certain processes in space or over time (e.g., Wu *et al.*, 2011, Ortiz-Karpf *et al.*, 2016, Reis *et al.*, 2016) when ages are constrained.

In such a context, previous studies tend to highlight only certain kinds of MTD features depending on the study. But to obtain a complete, objective description of an MTD, all its features need to be taken into account.

### 1.2. Interpreting MTD processes

From observed MTD seismic features, the processes related to physical failure suspected to play a role in the genesis of an MTD cannot always be quantitatively estimated. Thus, over-simplified interpretations based on descriptive approaches may come out (Vanneste *et al.*, 2014), whereas factual, verifiable relationships are required. In particular, an interpreter should take care when inferring local or too precise conclusions on slope-failure-related processes from statistical or conceptual relationships only. For instance, Urlaub *et al.* (2013) emphasize that the claimed link between sea-level change and mass movement triggering (and therefore the presence of MTD in a sedimentary unit) cannot be statistically inferred from worldwide MTDs – which does not mean it does not exist. Focusing rather on intermediate impacts (e.g. the impact of sea level fall on fluid migrations within the slope basement), which in turn affect slope stability, may make it possible to fit distinct responses of various environments. Unlike over-simplified interpretations, too precise ones may result in interpretations that are 'overfitted' to the seismic data. A balance thus needs to be found in the way the interpretation is made.

A failure event can be described by its triggering phase (possibly involving pre-conditioning environmental factors), its transport phase and its deposition phase (to which post-deposition processes may be added). The final (present-day) configuration of an MTD typically results from a variety of mass transport-related processes. One event may be generated by several causal processes (Richardson *et al.*, 2011), encompassing both the actual triggering factor and pre-conditioning

factors. Identifying one as the only triggering process is incorrect, as they may be mixed and interfere with each other both at temporal and spatial scales. The same is true for mass transport during the event: transport takes place at different scales (e.g. grain scale / flow scale); it involves several physical processes that are linked, even though modeling techniques tend to deal with one process at a time. Therefore, attempts to infer mass transport processes from MTDs should take into account the possibility of multiple influences, and also envisage the possibility of multiple interpretations before selecting the most probable one(s).

In all steps of an MTD characterization study (from the initial description to inferring mass transport processes), equivalently encompassing various kinds of processes and MTD features would increase the reliability of MTD interpretation. It would also enable objective comparisons. The principle of MTD classifications tends to oversimplify the description and characterization of MTD features and their causal mass transport processes. To date, the variety of physical processes involved in a mass movement, and the many seismic characteristics of their deposits, have not yet been integrated in non-oriented/agnostic seismic interpretation schemes. Such a scheme should take advantage of both existing knowledge (e.g. the literature) and seismic data specific to a case study, as two complementary sources of information.

### 1.3. Ontologies for inference problems in geological interpretations

Problems involving multiple data features of different kinds (e.g. quantitative and qualitative), multiple causal factors, and heterogeneous information sources, can be tackled by ontologies (e.g., Reitsma *et al.*, 2009). An ontology of a domain is an "explicit formal specification of the terms in the domain and relations among them" (Gruber, 1993). An ontology describes the domain exhaustively as a dictionary; it can be used as an inference engine with an adequate method to extract information from it. In geoscience for example, it can link several kinds of data and models, as done by Wang *et al.* (2018) who proposed an ontology on the 'local geologic time scale of North America, paleontology, and fundamental geology', together with a method to retrieve information from it. It can also convey the heuristic rules of inference of a domain; for instance, Verney (2009) presented an ontology for structural interpretation of a seismic cube.

Ontologies have methodological advantages. They help formalize and separate data-based and knowledge-based elements. They can be shared and improved as much as anyone wishes. They can be used in several ways. They yield repeatable results, and they can be automatized. An ontology could therefore be a relevant approach to the problem of inferring potential causal processes explaining MTD seismic features.

ACCEPTED MANUSCRIPT

### 1.4. Contributions and organization of this paper

In this paper, we build a knowledge base conceived as an ontology, which we consider an unbiased, standardized framework to convey the variety of features characterizing MTDs and their generating processes (section 2). We present a methodology for the interpretation of MTDs using this knowledge base. In this methodology, MTDs are considered as objects with representative properties, each one characterized by several features. These features are impacted by multiple physical processes, and these potential impacts are listed in the knowledge base. Our approach is an attempt to merge published results from a multi-disciplinary 'review', to enable the systematic comparison of several objects, while highlighting a variety of mass transport processes. We present an application of our methodology using 3D seismic data acquired offshore the Amazon River Mouth Basin (or Foz do Amazonas Basin, hereafter 'Amazon Basin'); the case study is presented in section 3, and the application of the methodology is detailed in section 4. The validity of our results is analyzed in section 5, and we discuss the global methodology in section 6. Our results enabled the validation of the methodology while revealing its limitations and possible enhancements.

Throughout this article, the event(s) at the origin of one MTD will be called (a) mass movement(s).

ACCEPTED MANUSCRIPT

# 2. Developing a new methodology for interpreting mass-transport processes from MTDs' seismic signatures

## 2.1. A new approach to an ontology

The methodology developed here relies on a global hypothesis: MTDs' observed characteristics are related to the processes that generated these objects, directly (one process acting on one observed characteristic) or indirectly (one process acting on another one, in turn affecting an observed characteristic).

We therefore have to consider an exhaustive description of MTD objects on the one hand, and an exhaustive description of the physical processes involved in the mass movement on the other hand. More precisely, the physical processes considered are those that act before, during or after the mass movement itself, and that may affect the mass movement; they may also be processes evolving at larger scale, associated with the regional or global environment (hereafter referred to as 'environmental controls'). Finally, we need to represent the possible impacts of one phenomenon (process) on an observed characteristic of the MTD, or on another phenomenon.

Here, we approach such an exhaustive representation of processes for geological object interpretation using an ontology. In our work, an 'MTD interpretation' ontology is a knowledge base containing information from this field of expertise, in the form of relationships, or laws, between key objects or concepts in the field. It is supposed to be exhaustive. The ontology is itself the set of objects (or concepts) and laws. The laws may be obvious, or heuristically accepted, e.g. 'arc-shaped pressure ridges on a MTD indicate a perpendicular flow direction' (e.g. Bull *et al.*, 2009). They may also be laws proven by numerical or experimental modeling, e.g. 'higher initial potential energy of unstable material yields higher runout distance for this material' (Mangeney-Castelnau *et al.*, 2005).

We build up our knowledge base as a graph (also termed relation map in this paper). A graph is a diagram consisting of a set of nodes together with edges joining certain pairs of nodes (Merris, 2001, Bondy & Murty, 2008). This representation shows how several objects / concepts, represented by nodes, are interconnected. It can also be represented in the form of an 'adjacency matrix', whose coefficients correspond to the connection between two nodes. In our case the nodes are physical processes of the mass movement, and are also their signatures termed 'MTD descriptors'. The word 'descriptor' is preferred to 'feature' as it conveys the notion of a description of an MTD property.

Edges can be either lines (for an undirected relationship) or arrows (for a directed relationship), in which case they represent the impact of one node on another (Figure 1 (a)).

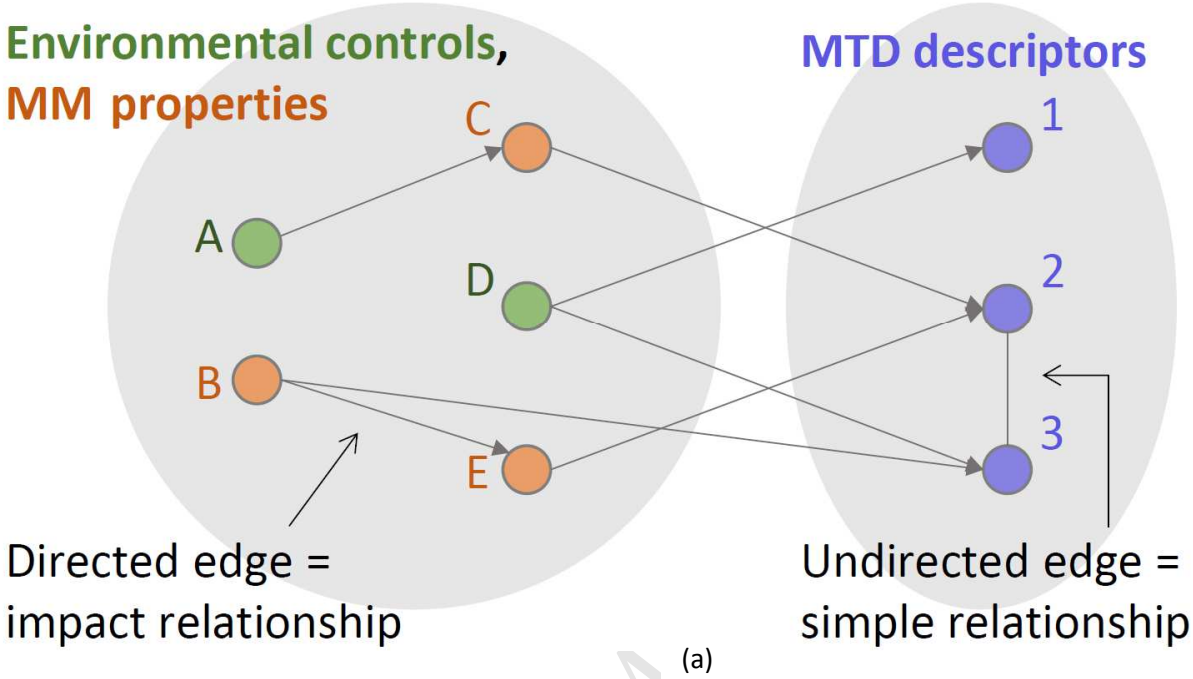


*Figure 1. (a) Schematic representation of our graph (relation map). Dots are nodes, colored according to their category (environmental controls, mass movement (MM) properties or mass transport deposit (MTD) descriptors); lines/arrows are undirected/directed edges. Interpretation of MTD descriptor 2 yields nodes C and E as direct potential impacting processes, then nodes A and B; node 3 is only related to node 2. (b) Representation of a sub-part of the global knowledge base, with nodes mentioned in the proposed application (section 4).*

ACCEPTED MANUSCRIPT

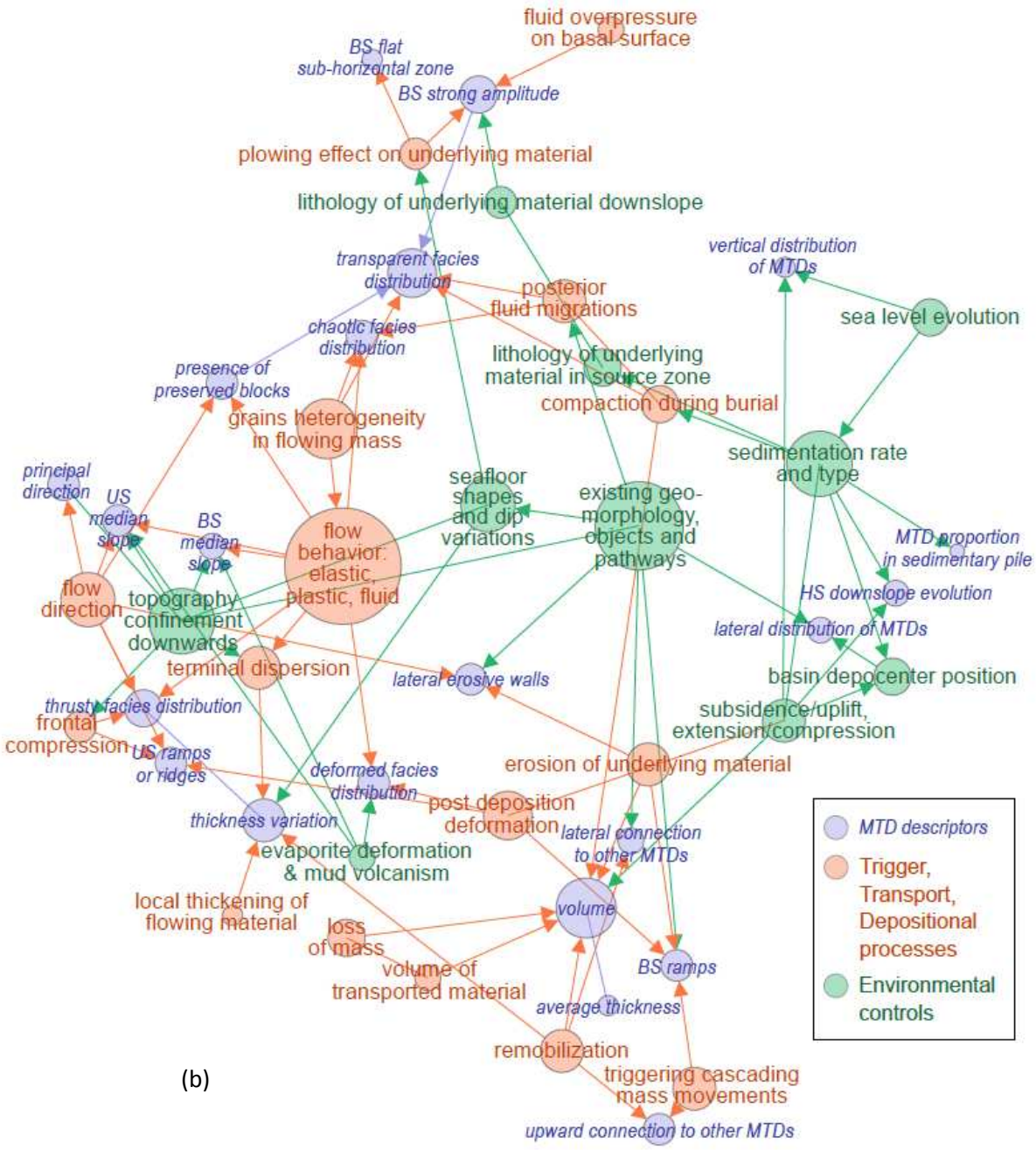


(b)

*(Figure 1 - continued).*

## 2.2. Building the relation map: nodes and edges from a bibliographical study

From a bibliographical study, we created a list of the most-relevant MTD descriptors (Table 1) that may be signatures of the mass movement characteristics, and a list of the most relevant phenomena (processes) (Table 2) involved in a mass movement. These two lists contain all the nodes of the graph.

We only considered works based either on statistical approaches to several well-known MTD cases, or on conceptual, numerical or experimental modeling (e.g. Mourgues *et al.*, 2014). Case studies were also used when their results were considered generalizable to other cases (e.g. Sutton & Mitchum, 2011). Each study considered focuses on one, or a series, of parameters controlling a mass movement and shows how (to a certain extent) these parameters impact specific MTD descriptors (e.g. volume, shape of the basal surface, presence of preserved clasts inside the MTD, etc.). We kept these parameters and the MTD descriptors to use as the nodes. Note that MTD descriptors and physical processes were filtered to keep only those that are relevant for interpreting seismic data. The bibliographical selection hopefully suffices to meet the exhaustiveness criterion needed for the knowledge base – this point could weaken our definition, but the bibliography can be increased whenever needed.

MTD descriptors were gathered into 7 groups (hereafter 'properties') that characterize an MTD as a geological object: Global Environment, Morphology, Position, Basal Surface, Upper Surface, Internal Facies Distributions, and Headscarp. All the descriptors (listed in the groups in Table 1) are global; they are either qualitative or quantitative. In the rest of this article, all MTD descriptors are written in *italics*.

| Properties | Morphology | Basal Surface | Upper surface | Position | Head scarp | Internal Facies Distributions | Global Environment |
|---|---|---|---|---|---|---|---|
| Descriptors | thickness variation<br>average thickness<br>width variation<br>horizontal aspect ratio<br>volume<br>surface area<br>maximum horizontal length<br>principal direction<br>presence of 'tongues' at toe | BS median slope<br>BS flat sub-horizontal zone<br>plunging pool indicator<br>multiple terracing downslope<br>BS ramps<br>scours, grooves or striations<br>lateral erosive walls<br>BS strong amplitude | US median slope<br>US ramps or ridges<br>US with turbidites on top | upward connection to other MTDs<br>lateral connection to other MTDs<br>near structural elements laterally<br>runout distance | HS downslope evolution<br>HS morphology | presence of preserved blocks<br>preserved blocks size<br>chaotic facies distribution<br>transparent facies distribution<br>faulty facies distribution<br>ridged facies distribution<br>thrust fault angle increase to toe<br>lithology distribution in MTD<br>deformed facies distribution | MTD proportion in sedimentary pile<br>lateral distribution of MTDs<br>vertical distribution of MTDs |

*Table 1. Characteristic properties of MTDs and their descriptors. BS: Basal Surface, US: Upper Surface, HS: Headscarp.*

Similarly, we gathered processes in two main groups: external, large-scale environmental controls at the time of the mass movement (e.g. sea-level curve trend, type of depositional environment, presence or not of confined topography), and physical properties of the event itself. The latter were divided into three sub-groups, according to the three phases that describe a mass movement: trigger-related, transport-related and deposition- (or post-deposition-) related properties. All the selected environmental controls and mass movement properties are listed in Table 2.

ACCEPTED MANUSCRIPT

225

ACCEPTED MANUSCRIPT

| | | |
|---|---|---|
| gravity, short term | Trigger phase | Mass movement properties |
| seismicity, short term | | |
| fluid overpressure, short term | | |
| offshore events and waves | | |
| chemical effects | | |
| flow velocity and energy | Transport phase | |
| flow behavior: elastic, plastic, fluid | | |
| local fluidization | | |
| local thickening of flowing material | | |
| volume of transported material | | |
| flow direction | | |
| modifying basin morphology | | |
| inducing seismicity | | |
| triggering turbidity current | | |
| triggering cascading mass movements | | |
| erosion of underlying material | | |
| plunging pool effect | | |
| plowing effect on underlying material | | |
| detached MTD | | |
| grains heterogeneity in flowing mass | | |
| fluid overpressure on basal surface | | |
| fluid overpressure in moving mass | | |
| initial potential energy of mass | | |
| lithology in transported mass | | |
| frontal compression | (Post-) deposition phase | |
| loss of mass | | |
| remobilization | | |
| compaction during burial | | |
| posterior fluid migrations | | |
| post deposition regional deformation | | |
| trigger turbidity current at stop | | |
| post deposition of turbidites | | |
| terminal dispersion | | |
| seismicity or waves, long term | | Environmental controls |
| evaporite deformation & mud volcanism | | |
| sea level evolution | | |
| basin depocenter position | | |
| subsidence/uplift, extension/compression | | |
| existing geomorphology, objects and pathways | | |
| sedimentation rate and type | | |
| pore pressure increase by compression | | |
| pore pressure increase by fluid migration | | |
| permeability increase | | |
| lithology of underlying material in source zone | | |
| initial aspect ratio and top of mass slope angle | | |
| topography confinement downwards | | |
| seafloor effective friction angle | | |
| seafloor shapes and dip variations | | |
| source domain in basin | | |
| lithology of underlying material downslope | | |

*Table 2. Environmental controls and mass movement properties. 'Mass movement properties' comprise properties of the trigger phase, the transport phase and the deposition phase (possibly including post-deposition modifications). 'Environmental controls' are large-scale processes.*

Finally, relationships between nodes were drawn to construct the edges, and were also extracted from the bibliographical study. Here, most of them are directed (arrow), representing the potential impact of one node on another. A directed edge may connect one process and one MTD descriptor, as a direct impact of the former on the latter; or it may connect two processes (two nodes listed in Table 2), thus allowing large-scale/conceptual/statistical controls to have an indirect impact on MTD descriptors through smaller-scale relationships. The list of edges is provided in supplementary material (Table_Supplementary 1).

### 2.3. Details and analysis of graph content

Here we first provide details on a few nodes (Table 1 and Table 2) and on the graph itself.

#### 2.3.1. MTD descriptors nodes

In the Morphology property, the descriptor *principal direction* corresponds to the principal orientation of the 3D geobody (in its current state, or inferred at the time of deposition if restoration has been performed). The descriptor *presence of 'tongues' at toe* is a binary indicator of whether some 'fingering' instability occurred at the front of the mass flow (typically triggered by grain size segregation), yielding a non-smooth toe region with 'tongues' (Pouliquen *et al.*, 1997, Woodhouse *et al.*, 2012).

In the Basal and Upper Surface properties, descriptor *median slope* includes the value of the slope median and its lateral variability over the MTD basal/upper surface, in order to capture typical relief while not taking into account fault- or ramp-induced extreme relief. *Ramps* are stair-like structures on basal or upper surfaces (e.g. Bull *et al.*, 2009). The *plunging pool indicator* is a reversed bell shape on a surface, associated with a hydraulic jump at a slope change in turbiditic systems, or with a unique high-energy mass movement that digs into the underlying sediment (Lee *et al.*, 2002, Bourget *et al.*, 2011).

The Headscarp property has two descriptors: *HS downslope evolution* indicates whether a series of headscarps are positioned gradually more basinwards with time (i.e. rising in the sedimentary deposits); *HS morphology* is a qualitative labelling of a headscarp between types 'onlap of upper surface on basal surface', 'cookie-bite', and 'unclear evacuation zone' (Richardson *et al.*, 2011, Dalla Valle *et al.*, 2013).

In the Internal Facies Distributions property, all facies distributions are typically described by their internal variations in the 3D space, comparing different regions within the geobody. The *ridged facies* is depicted by overlapping reflectors in the seismic data; whereas descriptor *thrust fault angle*

*increase to toe* is a binary indicator for cases with specific initial internal geometry or seafloor slope (Richardson *et al.*, 2011).

Note that all descriptors may not be available for all kinds of data/objects observed. In practice, two main limitations may prevent the availability of one or several descriptors: (i) if the MTDs and their corresponding headscarps are not entirely imaged within the seismic dataset used; (ii) if the data resolution is insufficient for Morphology, Facies and Environment precise descriptions, and if the surfaces needed were not picked with sufficient precision. First, to guarantee the detection of the top and bottom surfaces of an MTD, typically two reflectors, its thickness must be more than twice the seismic vertical resolution (ratio thickness/resolution > 2). When characterizing the MTD properties, more constraints apply. Facies descriptions within the MTD require a larger MTD thickness/resolution ratio: ~3 or higher, depending on the kind of facies (~3 for imaging deformed reflectors, ~5 for spotting preserved clasts within a matrix). This is more often the case for MTDs that are not too deeply buried (Alves *et al.*, 2014). Concerning surfaces, slope variations that allow description of ramps, for example, will not be seen if they occur at smaller scales than the precision of the picked surface. Morphological descriptors, as well as specific descriptors of the headscarp, or of the toe, of an MTD, require that these parts of MTDs be covered by the dataset. An estimation of the needed data quality for acquiring each input descriptor is provided in supplementary material (Table_Supplementary 2).

#### 2.3.2. Process nodes

Processes nodes (Table 2) are not thoroughly detailed here. We here only mention that, in Environmental Controls, ‘evaporite deformation’ and ‘mud volcanism’ were combined in one node to account for non-tectonic deformation in general, comprising mud volcanism, creep of evaporites, and even potentially diapiric movement of mud or salt (e.g. Moscardelli & Wood, 2008, Posamentier & Martinsen, 2011, Omosanya & Alves, 2013). The node ‘subsidence/uplift, extension/compression’ corresponds to large-scale tectonic or isostatic controls. Concerning the node ‘plowing effect on underlying material’ (*sensu* Posamentier & Martinsen, 2011), it implies reworking the sediments of the underlying stratum with the basal material of the flowing mass, capable of inducing compaction and dense deposition in the basal part of the mass.

Finally, there are no nodes for mass movement classes according to existing classifications (see e.g. those mentioned in the Introduction), since mass movement classes may differ from one classification to another, and since they do not correspond to actual processes.

#### 2.3.3. Graph analysis

Taking all nodes and edges together, the final graph built in this work (relation map) counts 88 nodes (38 MTD descriptors and 50 processes) and 173 edges. A full graph visualization is provided in Figure_Supplementary 1 (supplementary material), with a map of nodes and edges, and a representation of the adjacency matrix; this visualization illustrates the variation in the 'degree' (i.e. the number of edges connected to them) between nodes, by node size variation.

The 'degree' of the nodes is an analytical tool for graphs in general. Here (as also shown in Figure 1 (b)), it is not evenly distributed among nodes. Some processes (with a high 'degree') are therefore more likely to impact final MTD descriptors than others. These are the flow behavior (rather viscous or fluid), geomorphological objects and pathways already present at the mass movement time, sedimentation rate and type at that time, the presence of topographic confinement downwards, and the heterogeneity of the flowing material.

From the adjacency matrix of the graph, we highlight that no edge exists between trigger-related processes and MTD descriptors (no connection appears in the corresponding regions of the matrix). The impact of the former on the latter is indirect: trigger properties impact transport-related processes, which in turn impact MTD descriptors.

### 2.4. Methodology: how to use the graph (relation map)

As an ontology, our knowledge base can be used as an inference engine, i.e. to infer new results on potential causal processes from an applied case study.

The MTD interpretation methodology, relying on the graph, is divided into three steps:

- First, we characterize each MTD by a detailed description of its seven properties: for each property, we give a value to its quantitative/qualitative descriptors. Qualitative values are taken from data observation; quantitative values are obtained from a few computations on the data. Some edges guide the acquisition of descriptors, e.g. the description of 'lateral erosive walls' also includes whether they are seen on only one edge or on more, as this element is impacted by an edge. After this step, the MTD is characterized by 38 descriptors (Table 1) if all are available in the data.
- Then, for each descriptor, we look for all the edges (arrows) that point at it; possible controls or event properties (among those listed in Table 2) that may have an impact on the descriptor under consideration are given at the other end of these arrows. This corresponds to looking for the possible *causes of/explanations for* the descriptor's value. We note all the

possible 'causes' that the graph suggests, no matter how relevant they are with respect to other factors.

- Lastly, for each possible 'cause' listed in the previous step, we evaluate how uncertain it is: if the cause was found several times (i.e. if several descriptors pointed to it), then it is quite likely; if another cause was found that contradicts it, then it is highly uncertain, as is the other one. This implies that the *explanation* for some MTD descriptor might remain unsolved until cross-checking with one or several other descriptors. Thus, a result from the graph is obtained only when all available descriptors have been analyzed.

The final results of the relation map are not necessarily final interpretations, but rather hypotheses; the relevance of the methodology should be made explicit by the consistency between these hypotheses and available knowledge on the zone.

ACCEPTED MANUSCRIPT

# 3. Presentation of the Amazon case study

This section presents the geological settings of the region selected to test our methodology: the Amazon Basin. It also presents the data and material we used as inputs when applying the methodology.

## 3.1. The Amazon Basin and MTDs

The Amazon Basin sedimentation has been highly impacted by gravitational processes, at large and small scales (e.g. Reis *et al.*, 2010, Reis *et al.*, 2016, Silva *et al.*, 2016). Its geological history is closely related to that of the South-American continent. Since the onset of the Amazon River as a transcontinental river, believed to have occurred during the Miocene together with the Andean uplift (11.8 – 6.8 Ma, Figueiredo *et al.*, 2009), the river sediment discharge has kept increasing, progressively building up siliciclastic series on top of an in-place Cenozoic carbonate platform and in the basin. A deep-sea fan has developed farther from the continental shelf.

The current Amazon Basin is marked by large-scale gravitational deformation and several huge MTDs, marks of intense destabilization on the margin. These large MTDs have been documented and dated approximately; they are positioned in two zones: NW and SE from the main canyon axis (e.g. Reis *et al.*, 2010, Reis *et al.*, 2016, Silva *et al.*, 2016, Figure 2).

Smaller-scale MTDs are also visible, on or near the fan; some of them are definitely linked to basin-scale compression-extension processes. Globally though, the origin of these MTDs could be related to channel-levee complex instabilities on the deep-sea fan (Damuth & Embley, 1981), instabilities from fold-and-thrust belts on the deep-sea fan (Reis *et al.*, 2010), sea-level drop inducing gas-hydrate destabilization (Maslin *et al.*, 2005), and/or sediment collapsing under their own weight (Reis *et al.*, 2016).

## 3.2. MTDs in the NW part of the basin

Our study focuses on a sub-basin: the NW region of the basin, where the Amapá Megaslide (AM) has been studied and mapped by Silva *et al.*, 2010, Silva *et al.*, 2016 and Reis *et al.*, 2016 (Figure 2). AM consists of several mass transport complexes (MTCs): (1) The Amapá Lower Complex, (AM1 in Reis *et al.*, 2016) is the oldest (late Miocene) and probably results from the collapse of the mixed carbonate-siliciclastic platform; (2) the Amapá Upper Complex (comprising AM2 to AM6 in Reis *et al.*, 2016) is more recent (Pleistocene) and probably results from destabilizations of siliciclastic sediments on the marine slope favored by a regional décollement level – they were indirectly triggered by overpressure on this level on the deep-sea fan. The 50°W and Western MTD (also called Western

Debris Flows) are superficial MTDs (Figure 2), uncertainly dated 15 to 75 ka (Damuth & Embley, 1981, Damuth *et al.*, 1988). Both are associated with the deep-sea fan development and instabilities in the rapidly accumulated sediments on the fan flanks (Maslin *et al.*, 2005, Damuth & Embley, 1981).

In this paper, we analyze five MTDs observed in the basin of this NW region (see following section and Figure 3). Their lateral position covered by our seismic data (dark orange in Figure 2) is a few tens of km away from the sides of the Amapá Upper Complex and 50°W MTD.

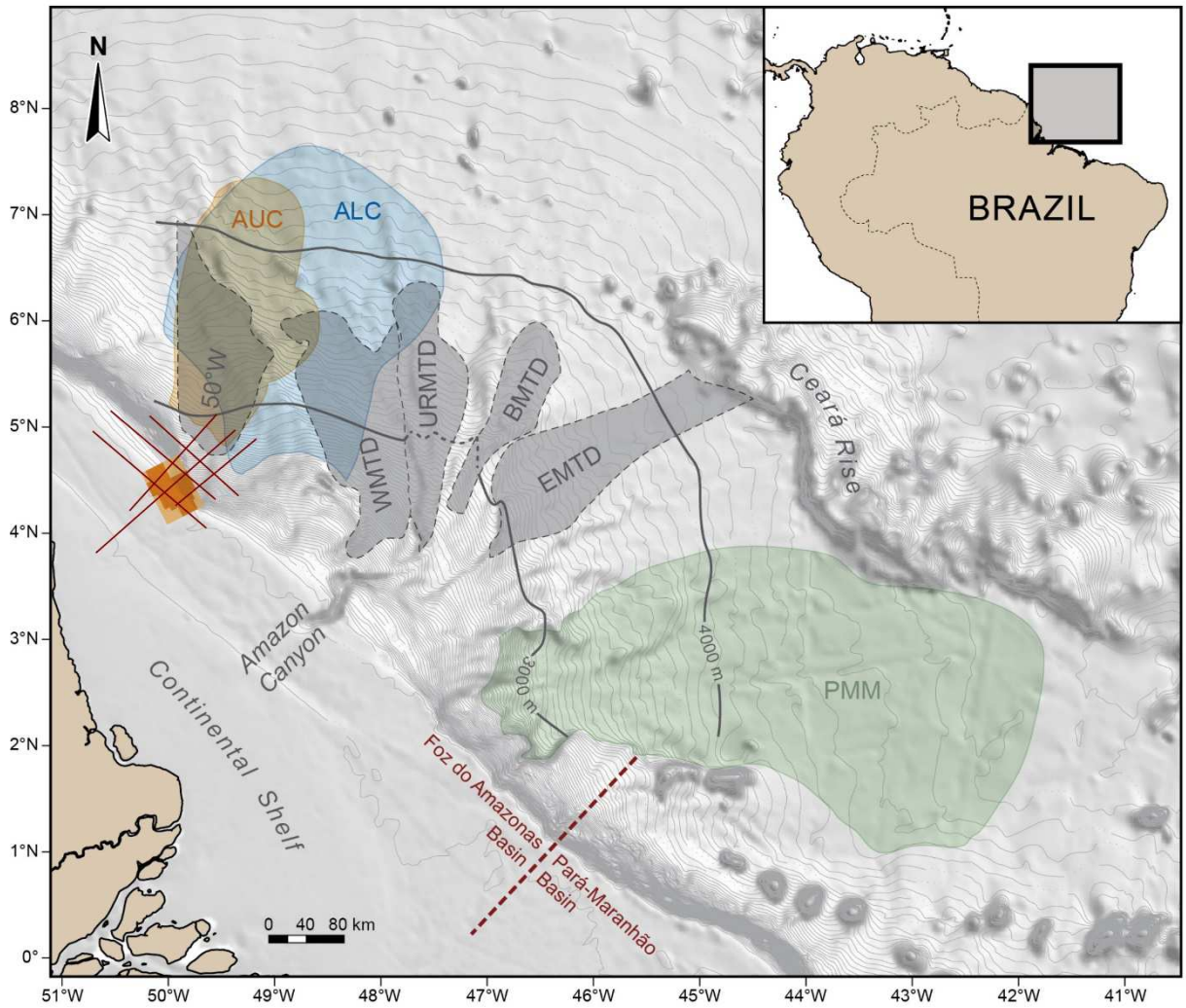


*Figure 2. Bathymetric map of the Offshore Amazon Basin with the location of major previously-studied MTDs and seismic data used in this article. Modified from Reis* et al.*, 2016 and Silva* et al.*, 2016. The 50°W (Damuth & Embley, 1981), WMTD, EMTD (Western / Eastern MTDs, Damuth* et al.*, 1988) are superficial MTDs. URMTD and BMTD (Unit R / Buried MTDs, Damuth* et al.*, 1988) are buried. The Amapá and Pará-Maranhão Megaslides (ALC-AUC / PMM) were studied by Silva* et al.*, 2010 and Reis* et al.*, 2016. Amapá Lower Complex (ALC), the deepest mass transport complex of Amapá, is mapped in blue; Amapá Upper Complex (AUC), more recent, is mapped in orange, after Reis* et al.*, 2016. The 3D seismic cube is mapped with available seismic data in dark orange and 2D seismic profiles are mapped in dark red.*

### 3.3. Data and materials – input descriptors for the methodology

Given the list of seismic MTD descriptors (Table 1), the mandatory data to test our relation map on MTDs in a seismic dataset consist of (i) basal and upper surfaces of each MTD delineated in the seismic data, (ii) position and headscarp descriptors of MTDs (contextual information), and (iii) seismic facies distributions for the seismic data and specifically for each MTD.

The seismic data used in this study is a post-stack time-migrated 3D cube granted by CGG Houston. The dominant frequency of the signal is 37 Hz, yielding a vertical resolution of 10 to 20 m (considering velocities from 1500 to 3000 m/s). The cube size is 60 x 43 km (2388 inlines, 1732 crosslines), with 25 m of intertrace; in this rectangle, data is only partially available (see dark orange in Figure 2). The cube is on the current shelf break with dip-oriented inlines, at the junction of three major domains: shelf, basin and deep-sea fan in the southern part. Upslope scarps were hand-picked in this cube and interpolated as surfaces using the GOCAD interpretation software.

For the MTDs description, a smaller cube was selected, in the deep Amazon Basin setting; it was restricted to a clastic sedimentary succession (2 sTWT thick) lying above the paleo-carbonate platform. The extent of our case study area was therefore 13 x 18 km, counting 512 crosslines and 710 inlines (see Figure 3). In this smaller cube, five observed MTDs were selected for analysis here. Their basal and upper surfaces were hand-picked on 72 inlines out of the 710 of the 3D seismic cube, using MATLAB and the GOCAD interpretation software. Figure 3 shows the MTDs, and upslope scarps, within the 3D seismic frame. The MTD thicknesses are ~50 ms in average, minimum 40 ms and maximum ~95 ms. The thickness/resolution ratio is therefore of 3 to 7.1 (for velocity of 1500 to 3000 m/s), which ensures the proper acquisition of input descriptors (see section 2.3 and Table_Supplementary 2). Among the five selected MTDs, MTDs A and B, which we analyze in more detail in the following section, are the deepest. They appear to be at the base of a seismic unit overlying a slope sedimentary series (Figure 4).

Comparisons of our analytical results with those of published seismic data rely on a few 2D seismic lines with 10-20 m vertical resolution, and a few previously-dated horizon surfaces provided by published material (e.g. Gorini *et al.*, 2014, Reis *et al.*, 2016). The horizons and seismic lines correlating with our seismic block made it possible to assess a stratigraphic constraint in the studied region; upslope scarps and downslope MTDs are all more recent than 2.4Ma.

We added our classification of seismic facies to the 3D input data. The classification, which was used as an input for this methodology, was made independently using a method developed by the IFPEN research group. A detailed discussion of the quality of this classification is beyond the scope of this

paper, but will be the subject of an upcoming paper. The classification, which resembles that of Roy *et al.* (2014), was applied as follows: (i) the data were clustered into most-similar regions, which led us to associate seismic facies labels to clusters of similar seismic properties; (ii) this procedure enabled us to label each sample of the seismic data with one or several names of seismic facies. Here we use the chaotic, transparent, deformed, strong-amplitude sub-horizontal, and ridged facies. They are detailed in Figure 5. Note that other facies descriptions (e.g. Alves *et al.*, 2014), if associated with seismic facies labels ('chaotic', 'deformed' etc.), could be used equivalently. The associations of facies labels with their descriptions have to be reliable and avoid pitfalls related to acquisition/processing footprints in seismic facies analysis (Marfurt & Alves, 2015). Note that the seismic facies defined in this way are not mutually exclusive, i.e. a region in seismic data may have a 'chaotic' facies and a 'transparent' facies at the same time[2]. Such multi-facies samples simply have several labels (e.g. chaotic and transparent) with no prevalence of one over the other.

Quantitative descriptors of the Internal Facies Distributions and of the Basal and Upper Surface properties were assessed within the MTDs and on their contours. The proportions of facies within MTDs were calculated, either by summing globally, or along a vertical or lateral direction. This enabled us to obtain maps or lateral variation plots, respectively. Additional information include the proportions of facies integrated over the 3D cube, and basal and upper surface gradient magnitude and direction, initially calculated using the time data and then assessed in °, a more practical unit, for a wave velocity range of [1500 to 3000 m/s].

[2] This is to be kept in mind for the analysis of results in terms of the proportion of facies in MTDs: the addition of the proportion of several facies inside a 3D object is not relevant.

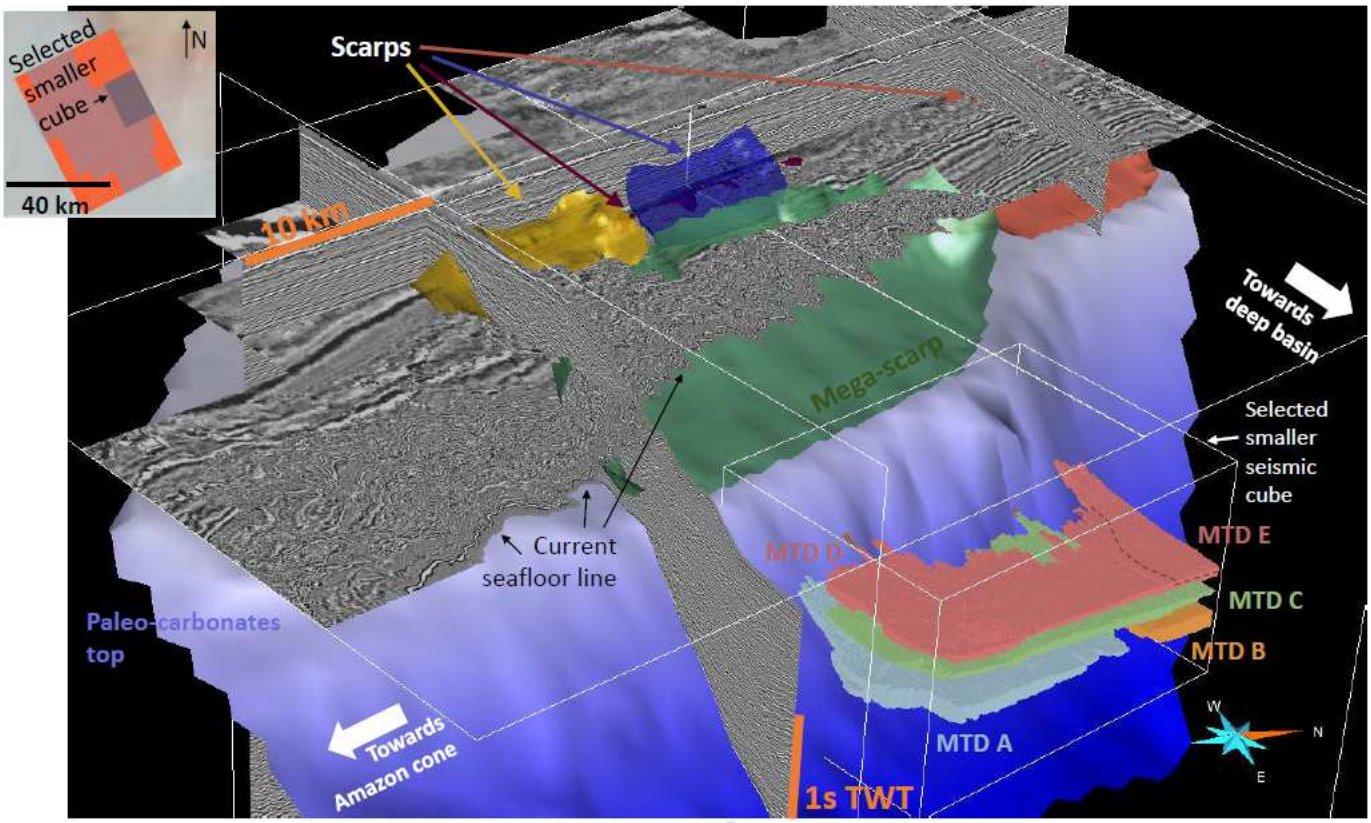


*Figure 3. 3D view of the five MTDs highlighted in the studied data. MTDs D and E are separated by the brown dashed line. Colored surfaces are upslope scarps. Grey sections are seismic sections from the seismic cube. The largest blue surface is the top of the carbonate platform (see also Gorini* et al.*, 2014).*

ACCEPTED

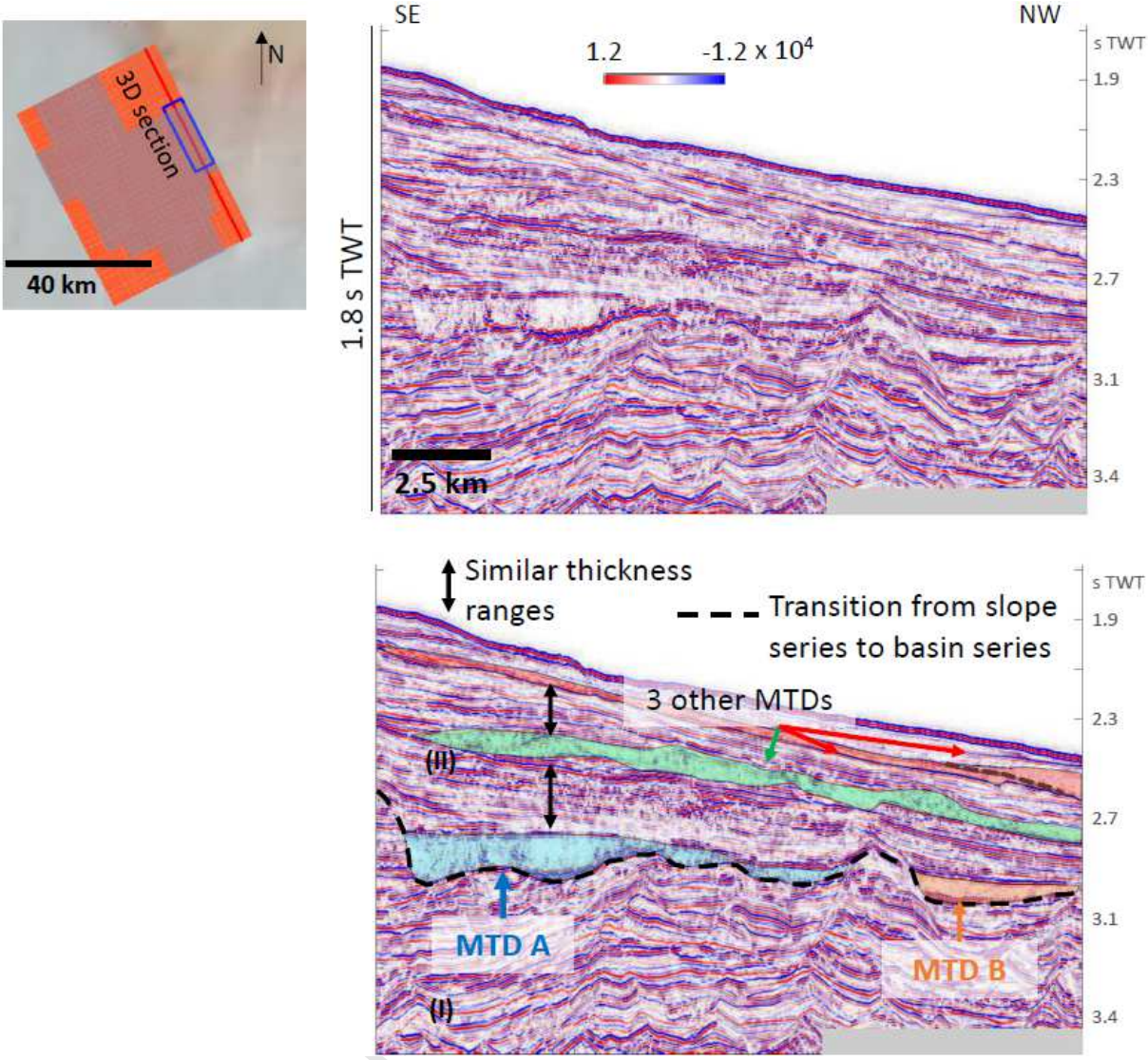


*Figure 4. The 5 MTDs highlighted in one seismic section of the post-stack seismic cube (uninterpreted and interpreted seismic sections). MTDs A and B appear to mark the beginning of seismic unit II above seismic unit I. The 3 stratigraphic periods for MTD deposition are separated by roughly similar thicknesses.*

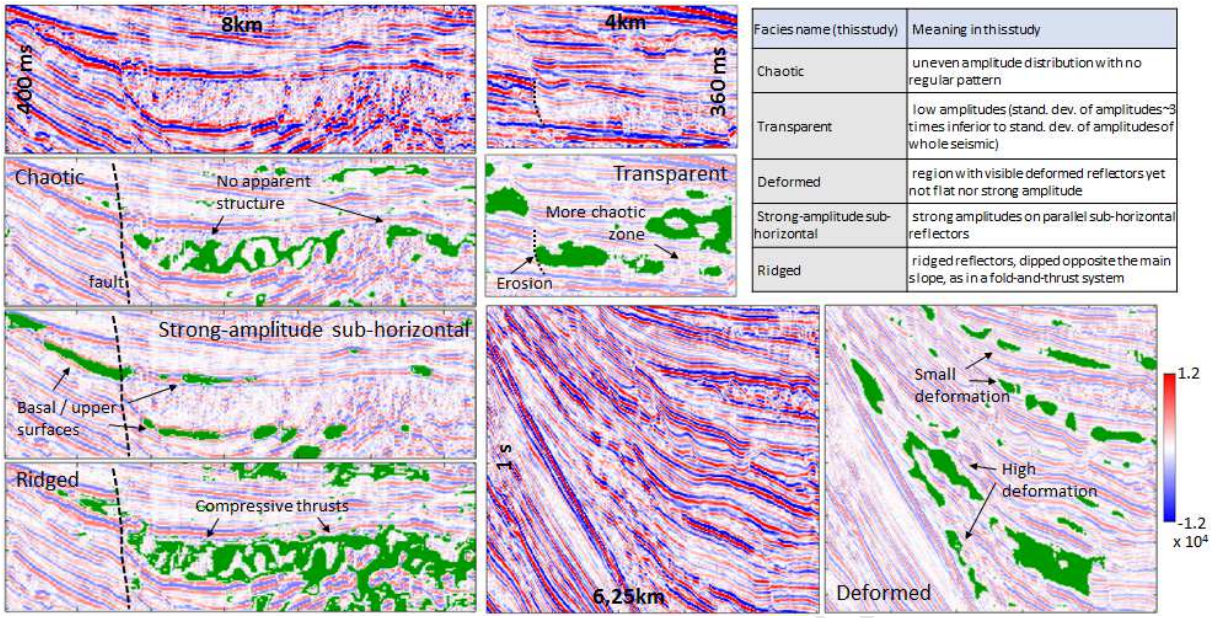


| Facies name (this study) | Meaning in this study |
|---|---|
| Chaotic | uneven amplitude distribution with no regular pattern |
| Transparent | low amplitudes (stand. dev. of amplitudes ~3 times inferior to stand. dev. of amplitudes of whole seismic) |
| Deformed | region with visible deformed reflectors yet not flat nor strong amplitude |
| Strong-amplitude sub-horizontal | strong amplitudes on parallel sub-horizontal reflectors |
| Ridged | ridged reflectors, dipped opposite the main slope, as in a fold-and-thrust system |

*Figure 5. Precise meaning ascribed to each facies used in this study, coupled with examples on seismic sections (shown as green patches on top of the seismic sections). Facies were interpreted based on an automatic method developed by the IFPEN research group, not detailed in this paper.*

ACCEPTED MANUSCRIPT

# 4. Application of the methodology to the case study

In this section, we describe how to use the relation map to derive a set of possible interpretations from MTD descriptors. We study the two deepest MTDs: A and B (Figure 3, Figure 4), among the 5 MTDs available and within the cube.

For MTDs A and B, for each of the 7 properties (Table 1) defined in our methodology, we retrieve associated descriptors (among those available in our data for these MTDs) and detail the steps of the methodology. Note that the relation map yields several hypotheses that are not final interpretations; they are possibilities, listed and estimated with the unbiased approach of the ontology – contextual knowledge should then help select most probable hypotheses. Figure 1 (b) illustrates this application with only the nodes mentioned in the text – the full graph is available in Figure_Supplementary 1 (supplementary material).

## 4.1. Global Environment

The Global Environment property has a few descriptors, which here concern the series of five MTDs (Figure 3). In our small seismic cube, the calculated global *proportion of MTD-delineated sediments* in the recent sedimentary series is 9%.

The *vertical distribution* of our five MTDs shows three main stages of deposition of sedimentary bodies (as two pairs of MTDs are in the same stratigraphic level). Firstly, this *vertical distribution* yields the relative age of all MTDs: MTDs A and B are the oldest. Secondly, the three main stages of sediment disruption are separated by a roughly similar thickness of sediments (Figure 4). According to the relation map, this vertical (almost) cyclical deposition could correspond to sea-level cycles (node 'sea-level evolution' impacting descriptor *vertical distribution*) – if the MTD stages are interbedded with channel-levee systems (Sutton & Mitchum, 2011), which is not obvious from the data only. Alternatively, tectonic- or isostasy-related large-scale deformation could explain this vertical distribution (impact of the node 'subsidence/uplift, extension/compression'). Within the stages with two MTDs, the nodes 'existing geomorphology, objects and pathways' and 'basin depocenter position' may impact the *lateral distribution* of MTDs, showing potential influences of the seafloor shape. The absence of MTD in the south-eastern part of the cube suggests that throughout this period of clastic deposition, the sub-basin depocenter was never located in that part – but instead more basinwards, or more to the north-west; or, that the sub-basin south-eastern geomorphological conditions made it less exposed to mass-transport deposition.

## 4.2. Morphology

Descriptors depicting the property Morphology are now highlighted, with a specific focus on MTDs A and B.

The *average thicknesses* of MTDs A and B, 97ms and 90ms respectively, are the largest of all five MTDs identified in the seismic cube. On the relation map, the *average thickness* node is related to the 'volume' node, which in turn is impacted by several nodes concerning transport- and deposition-related processes, such as: 'volume of transported material' (quantity of material), 'loss of mass', 'erosion of underlying material', 'compaction during burial', and 'remobilization'. Considering that these MTDs are the oldest ones in the stratigraphic succession studied, they are the most likely ones to have been modified after deposition (by compaction); this suggests that when they were deposited they were even thicker compared to the other MTDs. Moreover, 'loss of mass' during the event itself, or subsequent remobilization, would have decreased the final quantity of deposited material compared to the initially-destabilized mass. As for process 'erosion of underlying material', it could decrease or increase the material quantity depending on the kind of erosion, which is not known for now. Therefore, the initial volume of sediment that was transported to generate MTDs A and B was probably equal to, or greater than, the current MTD volumes.

While MTD B is consistently thin on its upper sides and thickens downwards, MTD A has two distinct thicker zones. From the relation map, we know that node *thickness variation* is impacted by the nodes 'remobilization', 'frontal compression', 'local thickening of flowing material', 'terminal dispersion', and 'seafloor shapes and dip variations'. According to the relation map then, thicker MTD zones may be related to (i) pre-existing depressions in the seafloor (see e.g. Sawyer *et al.*, 2012, Mulder & Alexander, 2001a and Table_Supplementary 1); or (ii) to a local thickening associated with ductile flow of the basal material (shown for sandy flows by Mourgues *et al.*, 2009); or (iii) to thrust-induced elevations of the upper surface. Further analyses on other properties should help limit possible interpretations. As for the 'terminal dispersion' and 'remobilization' nodes, they would cause thinning (rather than thickening), which is not the case here; thus for now, we do not retain them as potential impacting processes.

Other descriptors of the Morphology property are not available due to the limited surface area covered by our data. Nevertheless, we note that the *principal direction* descriptor (i.e. principal orientation of the 3D geobody) is impacted by the nodes 'flow direction' and 'topography confinement downwards'. For MTDs A and B, the *principal direction* is NNE, rather than ENE which is the basinward direction. One of the two above mentioned processes could thus have influenced the deposit *principal direction* that eventually became distinct from the main slope dip direction – but

these interpretations are uncertain, due to the limited data available for *principal direction* assessment.

### 4.3. Position and Basal Surface (BS)

For both MTDs A and B, *lateral erosive walls* only occur along their southern limits, as highlighted on their basal-surface gradient map (Figure 6). The *lateral erosive walls* descriptor is impacted by nodes 'erosion of underlying material', 'flow direction' and 'existing geomorphology, objects and pathways' (Bull *et al.*, 2009, Moscardelli & Wood, 2008). These erosive walls are identified on the southern flank only; they are not aligned with the *principal direction* of the objects. These elements show a probable impact from node 'existing geomorphology, objects and pathways', which were therefore probably not symmetric with respect to the main flow direction at the time the event occurred; the 'flow direction' must have been modified from the ENE (main slope-dipping) direction to a NNE direction, thereby eroding the neighboring material.

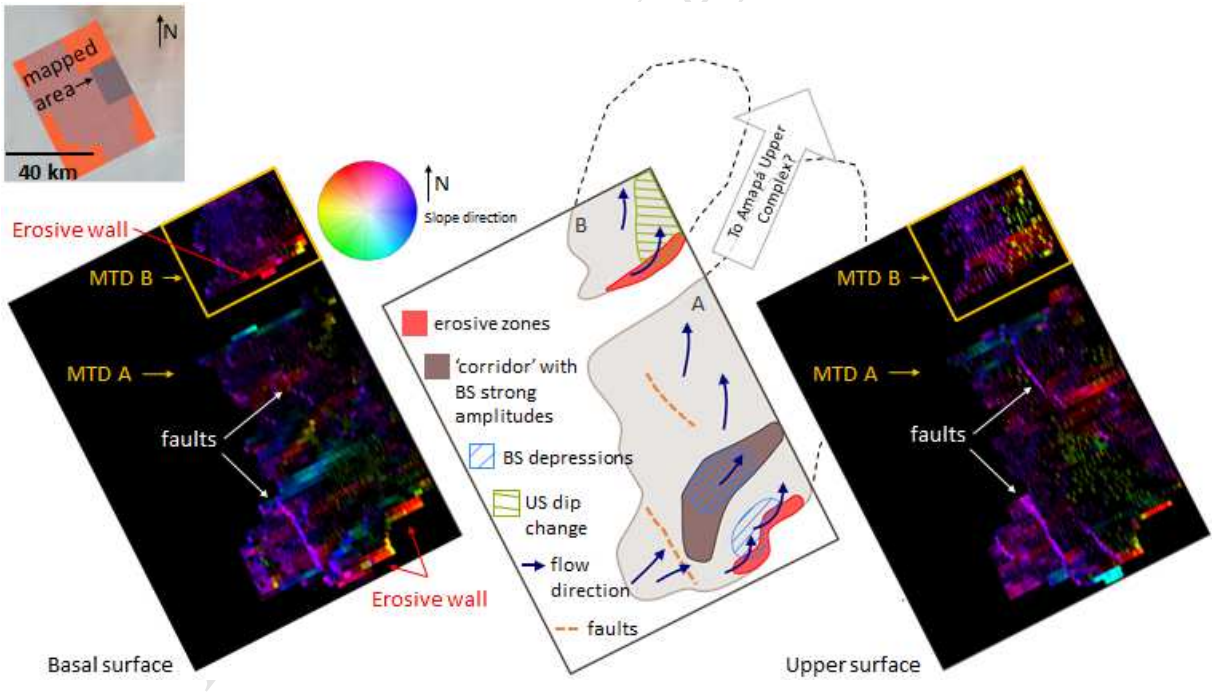


*Figure 6. MTDs A and B slope maps of basal surfaces (BS) and upper surfaces (US). Dip direction shown by color hue, dip value by brightness. Both MTDs show a lateral erosive wall in their BS southern regions, and a change in BS and US dip orientation, indicating a change in orientation of the flow. Faults are visible on the BS and US of MTD A. Interpreted map shows a strong amplitude 'corridor' and two topographic depressions of the BS, retrieved from amplitude and topographic maps respectively. Amapá Upper Complex is described by Reis et al. 2016 (see Figure 2).*

MTDs A and B are separated by ~500m laterally and underlined on the seismic sections by a common reflector (basal surface BS), thus implying events occurring in the same time period. The *lateral connection to other MTDs* descriptor may be impacted by the node 'remobilization' – suggesting on the one hand that MTD B was made of material remobilized from A –, and node 'existing geomorphology, objects and pathways' – suggesting on the other hand that MTDs A and B result from a single mass movement, whose deposit was separated by a topographic high downslope; note that these possible impacts are contradictory. Now, an *upward connection to other MTDs* is also observed, as the upper part of MTD B is located ~20msTWT above the lower part of MTD A. This *upward connection to other MTDs* node is impacted by the nodes 'triggering cascading mass movements' and 'remobilization' (which, given their spatial relationship, would be from MTD A to MTD B). Process 'remobilization' is enhanced as it appears for the second time. However, based on what was proposed ~~before~~ above (see Figure 6 and comments on the 'lateral erosive walls'), the material of MTD B originates from the WSW and not from MTD A (SE). So, considering the remaining possible processes impacting the *lateral* and *upward connection to other MTDs*, MTDs A and B are probably either signatures of one single event (eventually separated because of pre-existing topography) or cascading events (whose sources were close to each other, failure of MTD A triggering mass movement B).

While the basal surface of MTD B has no *BS ramps* and its *slope* is quite regular, from ~-1° to max. [-2.5° to (-5)°], BS *slope* of MTD A varies from [-5.5° to (-11.5)°] upslope, to +1° downslope, and is affected by *ramps* (Figure 7 – see similar examples in Richardson *et al.*, 2011). *BS ramps* are signatures either of node 'triggering cascading mass movements', or of node 'post-deposition regional deformation', or of node 'erosion of underlying material', or yet of node 'existing geomorphology, objects and pathways' suggesting pre-existing ramps on the paleo-seafloor (e.g. Richardson *et al.*, 2011, Mienert, 2009, Frey-Martínez, 2010). Thus, these four processes are more likely to have occurred in MTD A than in MTD B. Further arguments from analyses on other descriptors/properties should favor one among these four.

The Basal surface (BS) of MTD A also comprises two deeper zones, or depressions; these account for the previously mentioned variations in thickness. In these depressions, the BS has a *flat sub-horizontal* trend. This *BS flat sub-horizontal zone* descriptor may be the signature of a 'plowing effect on underlying material' (Posamentier & Martinsen, 2011, see also section 2.3). This process seems here to be more likely in the two depressions of MTD A. The local variations in thickness analyzed in 4.2 can be explained by either (i) pre-existing depression in the seafloor or (ii) local thickening associated with basal ductile flow, rather than thrust-induced elevation of the upper surface (iii).

MTDs A and B are both characterized by the descriptor *BS strong amplitude*. Descriptor *BS strong amplitude* is impacted by the nodes 'lithology of underlying material downslope', 'fluid overpressure on basal surface', and 'plowing effect on underlying material'. In turn, the node 'lithology of underlying material downslope' is related to the node 'lithology of underlying material in source zone'; this indicates that if the medium is homogeneous between the source and deposition regions, then the impedance contrast observed at a *strong-amplitude* basal surface should be explained by a change in the MTDs' basal material rheology. In MTD A, one current topographic depression shows very high amplitudes, with a negative polarity (Figure 7), whereas in MTD B the polarity of the *BS strong-amplitude* region is positive. Based on the relation map then, two scenarios may explain these differences:

- MTDs A and B have similar acoustic impedances, but their respective underlying material has lower impedance in the south-east (under A) than in the north-west (under C). This could be linked with the occurrence of some degree of fluid overpressure along the BS of MTD A.
- The underlying material shared by MTDs A and B has uniform acoustic properties, but the material of MTD B results in lower acoustic impedance than that in MTD A. As the material of MTD B probably does not originate from remobilized material from MTD A, the difference would then be due to different transport properties of the mass movement (either of the two 'branches' of a single event, or of the two cascading events). For instance, a plowing effect occurring in event A would lead to reorganization of its basal sediments, thereby densifying the bottom of the MTD in one topographic depression (see 'corridor' in Figure 6).

Here, the relation map enables two possible main interpretations that remain to be ranked depending on further arguments provided by other properties or from posterior contextual information.

ACCEPTED MANUSCRIPT

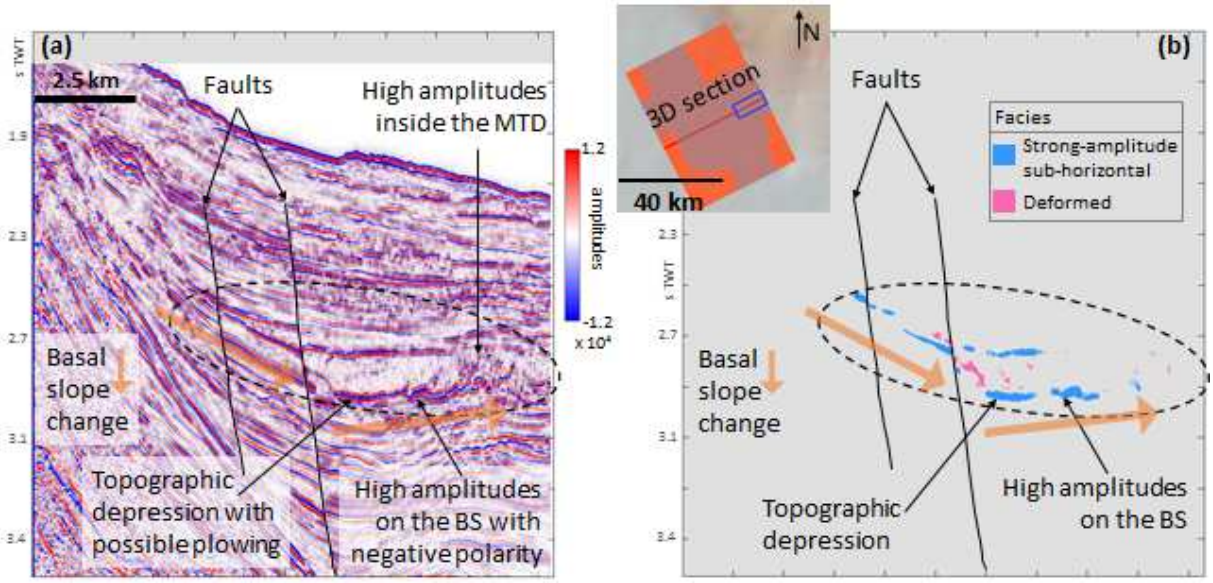


*Figure 7. MTD A (dashed circle). Seismic section (a) and seismic facies (b). Faults and topographic depression are highlighted, with possible plowing (sensu Posamentier & Martinsen, 2011) on the high-amplitude negative-polarity basal surface (BS) of MTD A. Irregular high amplitudes are also visible inside MTD A. Deformed facies rather appears at the head part of MTD A (similar distribution for C).*

### 4.4. Upper Surface (US)

On MTD A upper surface (US), *ramps* similar to those ~~as~~ on its BS are visible. According to the relation map, descriptor *US ramps or ridges* is impacted by the nodes 'post-deposition regional deformation', 'frontal compression' and 'flow direction' – very different kinds of processes. Here, however, it is possible to select the most likely: the BS and US *ramps* coinciding on MTD A favor their common impacting node ('post-deposition regional deformation'), indicating signatures of a faulting deformation of the MTD after deposition (Figure 6, Figure 7).

The Upper surfaces (US) of MTDs A and B both have a *median slope* gradient of [-1° to (-2°)]; this value is much lower than the *median slope* gradient of their basal surface [-3.5° to (-7°)]. Descriptor *US median slope* is impacted by the nodes 'flow behavior: elastic, plastic, fluid', 'flow direction', 'topography confinement downwards', and 'evaporite deformation and mud volcanism'. A significant dip change is visible on the US of MTD B (Figure 6)-that may be related to the nodes 'flow direction' and 'topography confinement downwards'; it correlates with the change in the orientation of the object (see 4.2). In this area, the *US slope* is an additional argument for the occurrence of a change in flow direction. On the other hand, the 'flow behavior: elastic, plastic, fluid' node may explain the lower *median slope* gradient on the US than on the BS; this is to be compared to the [-1.5° to (-3.5°)] *median slope* gradient of two other MTDs of the same cube (MTDs C and D, Figure 3), and to the current seafloor *slope* of [-1.5° to (-3°)] in the downslope part. The low *US median slope* of MTDs A and B thus suggests the occurrence of a rather 'fluid' flow, compared to that of other MTDs of the cube with inferred more 'viscous' flows.

### 4.5. Internal Facies Distributions

As a whole, MTDs A and B are 12% and 11% *chaotic* respectively, with internal variations: both are mostly *chaotic* in their southern part. *Ridged facies* are similarly distributed inside MTDs A and B, with an overall 30% proportion of occurrence for both. Descriptor *chaotic facies distribution* is impacted by the nodes 'flow behavior: elastic, plastic, fluid', 'grains heterogeneity in flowing mass', and 'posterior fluid migrations'; *ridged facies distribution* is impacted by the nodes 'frontal compression ', 'flow direction' and 'flow behavior: elastic, plastic, fluid'. These elements show that for both mass movements A and B, when arriving in the northern part, the material probably had a different flow behavior than that in the southern part (consistency of the 'flow behavior' node for both descriptors). A change in compression constraints and flow direction between south and north is also in line with the previously-mentioned orientation change of the objects. According to the other above-mentioned impacting nodes, additional possible interpretations for both MTDs A and B are: increased homogeneity in the acoustic properties of the material in the northern part, and post-deposition uneven fluid migrations occurring inside the southern part of the MTDs.

The *deformed facies* proportion of MTD A is quite low, only 2%, whereas for B it is 11%. For both of them, *deformed facies* are seen at the contact between the upslope part of the MTD and their underlying material (Figure 7 (b)); and notably MTD A is 10% *deformed* in its upper part but <5% *deformed* everywhere else. The *deformed facies* descriptor is impacted by the nodes 'flow behavior: elastic, plastic, fluid', 'post-deposition regional deformation', and 'evaporite deformation & mud volcanism'. Thus, for both MTDs A and B (with more quantitative arguments for A), deformation occurred more on the bottom of the head part, either due to a particular flow behavior there, or to post-deposition regional deformation, or to local evaporite- or mud-related deformation in the zone.

MTDs A and B have different *transparent facies distributions*: MTD A is only 11% transparent on average, while MTD B is 28% transparent. However, MTD A is >20% transparent inside its two thicker regions; other interior parts of MTD A have unevenly-distributed high amplitudes, roughly aligned with the fractured BS patterns (Figure 7). Descriptor *transparent facies distribution* is impacted by several nodes: 'grains heterogeneity in flowing mass', 'compaction during burial', 'posterior fluid migrations', and 'presence of preserved blocks'. The high-amplitude region inside A (low proportion of *transparent facies*) may correspond to either preserved clasts (of size ~1/3 of the MTD thickness), or to over-pressured fluids heterogeneously trapped inside the MTD, migrating after its deposition or remaining from an undrained mass transport. Comparatively lower amplitude (transparent) zones in MTDs A and B would then correspond to regions with more internal homogeneity, possibly enhanced by compaction or homogenized fluid drainage during burial.

### 4.6. Headscarp (HS)

The multiple *headscarps* visible upslope are possibly related to downslope MTDs; however no direct relationship can be identified between one single MTD (among the five seen in the cube, see Figure 3) and one upslope scarp – preventing us from analyzing descriptor *HS morphology*. Yet these *headscarps evolve downslope* (Figure 8); this description suggests the impact of two controls: some large-scale 'subsidence/uplift, extension/compression', in the zone (inducing a progradation of sedimentary structures, as in, for example, Richardson *et al.*, 2011, Ortiz-Karpf *et al.*, 2016, Clark & Cartwright, 2009), and/or 'sedimentation rate and type' (in the sense of a sedimentation increase with time), according to the relation map. The period of time in which these scarps were created is from 2.4Ma to present (Gorini *et al.*, 2014, see Figure 8). Knowing the rate of tectonic or isostatic deformation since 2.4Ma would make it possible to constrain a potential impact on this evolution. Similarly, as the node 'sedimentation rate and type' is itself impacted by the sea-level evolution, knowing this time more precisely could help confirm or invalidate a eustasy related headscarp series, and also the above-mentioned MTD *vertical distribution*. The relation map based results do not favor either of these two interpretations.

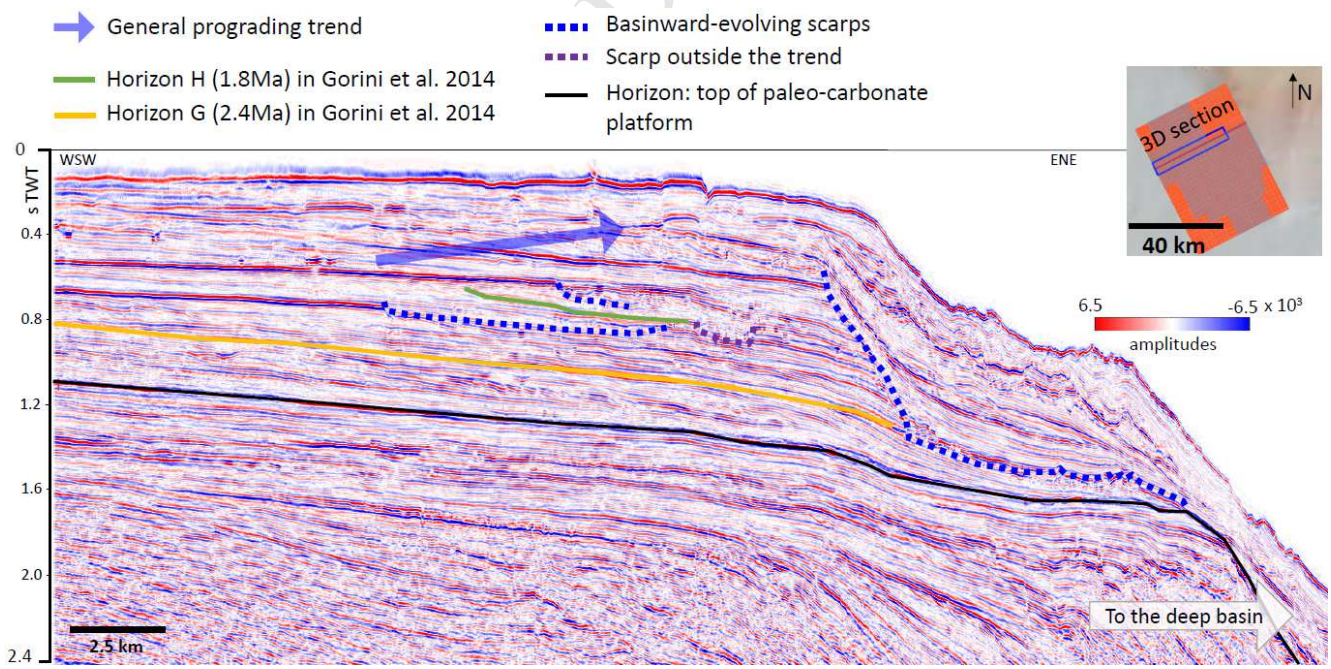


*Figure 8. Upslope scarps showing fore-stepping evolution of the erosion on one dip seismic section from our seismic cube.*

### 4.7. Summary of all results retrieved through the relation map analysis

The material of MTDs A and B probably originates from the WSW (rather than from the south), and both MTDs are probably signatures of a single event, or cascading events (one mass movement triggered by the change in slope stability induced by the other mass movement). MTD A is more likely to have been subject to post-deposition regional deformation, in the form of extensional faults, than MTD B.

Both MTDs may have resulted from more fluid-like material flows than the other MTDs of the same cube. A plowing effect may have occurred during mass movement A, more likely located in one of the two observed topographic basal depressions; furthermore, right above the deepest part of these depressions, the acoustic properties of MTD A are relatively homogeneous. Preserved clasts or trapped/undrained fluids may be found in other parts of its southern region. Deformation occurred more in the bottom head part of MTDs A and B, due to either a more viscous-like basal flow, or to post-deposition deformations.

For MTDs A and B, the flow direction during the event was modified in its distal part. The flow behavior of their material probably differed in the southern parts of both MTDs from that in their respective northern parts. In particular, compression and/or post-deposition uneven fluid migrations may have impacted the southern part of MTD A – compression is more obviously related with a change in orientation, corresponding to a topographic impact. In their northern parts, a greater homogeneity in MTDs acoustic properties is found, suggesting more homogeneous distribution of material properties at the time of deposition, and/or homogenization by posterior compaction effects or homogenized fluid drainage (during burial).

Two possible processes may explain the difference in polarity between the basal surfaces of MTDs A and B (in places where the basal surface has strong amplitude): either a lower impedance of the underlying material in the south (possibly including some fluid overpressure on the contact surface); or the two 'branches' of a single event (or the two cascading events) with different transport properties, e.g. a possible plowing effect in mass movement A densified its bottom sediments during deposition.

Concerning more general aspects, the three main stages of the "MTD layers" in the stratigraphy may be signatures of eustatic cycles – if other alternating systems like channel-levee systems are detected in the sedimentary pile, which is uncertain in our data. Some regional deformation due to tectonics or isostatic movements, inducing global progradation and/or sedimentation rate increase, may have

ACCEPTED MANUSCRIPT

occurred during the whole period when the 5 MTDs were deposited. And finally, the southern part of the cube was less exposed to mass-transport deposition during this period.

ACCEPTED MANUSCRIPT

# 5. Assessing the validity of results

In this section, we analyze the correlation between results based on our proposed relation map and previous published studies on the Amazon Basin.

## 5.1. To what extent are our results consistent with previous knowledge on the Amazon Basin?

Our seismic dataset is located in a very proximal region of the Offshore Amazon Basin (~120 to 1500 m deep), close to the upslope domain of the Amazon deep-sea fan. This region corresponds to the junction between the current shelf break, the Amazon deep-sea fan and the area affected by the Amapá Megaslides Complex (Figure 2). In the present study, we analyzed cube-scale MTDs (a few tens of km). Previous studies of the northern part of the basin focused on much larger, basin-scale MTDs (a few hundreds of km), observed on 2D seismic data. In their studies, Gorini *et al.* (2014), Reis *et al.* (2016) and Silva *et al.* (2016) propose an age spanning from late Miocene to late Pleistocene for different MTDs of the Amapá Upper Complex. These basin-scale MTDs typically originated from marine slope instabilities. Maslin *et al.* (2005) focused on Quaternary MTDs of the 'Western Debris Flows' complex, considered as typical MTDs induced by the development of the deep-sea fan (Figure 2). These two kinds of MTDs characterize the entire basin sedimentation.

Thus, the MTDs characterized in this paper are at a much smaller scale than those previously studied across this basin. Nevertheless, our results show the consistency between the results of the analysis based on the relation-map and the known context of the Amazon Basin.

First, we know that MTDs in the northern Amazon Basin region, resulting from mass movements dated from the late Miocene to Present, are mostly debris flow signatures. General classifications define debris flows as being composed of a matrix containing internal blocks (Nelson *et al.*, 2011), resulting from 'spreading' (*sensu* Mourgues & Cobbold, 2006) or from 'mixed plastic-fluid' flow (*sensu* Posamentier & Martinsen, 2011), that still retains some competence and not being as energetic as a turbidity current (Lee *et al.*, 2007).

The MTDs we studied are at most a few Ma old, corresponding to the same period of deposition as the Amapá Upper Complex (Reis *et al.*, 2016) and the superficial MTDs described in the literature (e.g. Damuth & Embley, 1981, Damuth *et al.*, 1988, Maslin *et al.*, 2005). A few elements on MTDs A and B are in line with the interpretation of a debris flow type: (i) homogeneous acoustic properties (with low impedance contrast), alternating with heterogeneous regions where either clasts or fluids may be trapped. (ii) The overall limited presence of deformed facies reveals a very limited plastic

deformation, which is characteristic of material flows rather than of slides or creeps (Posamentier & Martinsen, 2011) in which deformation plays an important role. (iii) Erosion signatures can be generated by debris flows, although slides can also erode their underlying material. Here, the erosion marker is located at a change in the direction of the material displacement, and some compression has left marks inside the MTDs; this tends to favor debris flow behavior rather than slide behavior.

Second, we know that the entire Amazon Basin is subject to 'gravity-tectonic' deformation (Reis *et al.*, 2016), which produces extension in its proximal part, and distal compression. The faults observed on MTD A could be a sign of the proximal extensional constraints – although they are possibly also linked to surficial compaction. Why they are not visible on MTD B is either linked to the (slightly) more distal position of MTD B (4-6 km more distal), or to the position of A closer (~10 km) to the edge of the deep-sea fan – generalized faulting in the southern part of the seismic cube seems to favor this argument. This leads us to the third point.

Third, results based on our relation map on MTDs A and B seem to be consistent with the presence of the deep-sea fan just south-east of the studied seismic cube (Figure 2). It has been shown that this deep-sea fan has created three major kinds of influences since its onset in the Middle-Late Miocene (Figueiredo *et al.*, 2009; 9.5 – 8.3 Ma according to Gorini *et al.*, 2014): acting as <u>a secondary source</u> of sediments for transport into the deep basin (e.g. Reis *et al.*, 2010, Maslin *et al.*, 2005, Araújo *et al.*, 2009), having <u>topographic control</u> over the seafloor shape, and <u>structural control</u> (Watts *et al.*, 2009) by flexuring the margin under its weight.

In our study, MTDs A and B are shown to originate from the paleo-shelf break; yet their direct environment may have been impacted by the presence of <u>sediments coming from the fan direction</u>, as suggested by the difference in BS polarity between MTDs A and B that were deposited either simultaneously or within a short period of time. Over such a short distance between the two MTDs, a local process (such as the presence of fluid, or locally different material properties) probably explains this inversed polarity. Post-deposition compaction, and/or fluid migrations preventing efficient drainage from the BS of MTD A, could explain this difference, e.g. in the case of fluid present under MTD A (hypothesis that would be supported by the presence of fluids *inside* A too). Alternatively, near-fan sedimentation may be subject to different deposition conditions; these may include different sediment inputs, transported via contouritic currents around the fan or turbiditic currents originating from the fan that, mixed with recently deposited sediments downslope, would eventually yield lower-impedance sediments. This hypothesis is supported by the BS polarities of other MTDs of the cube, which are always negative in the southern region (close to the fan) and positive in the north – assuming the influence of the fan has remained similar since the deposition of MTDs A and B.

The topographic control is highlighted in our results via the change in flow direction in MTDs A and B, which may be evidence for a topographic constraint. The deep-sea fan itself is an accumulation of material that creates a NW-dipping slope in the seafloor, already present at the time of deposition of MTDs A and B. The debris flows probably changed their main direction from dip-oriented (originating from the WSW) to more northward-oriented, i.e. following the main slope direction in the more distal region of the cube, impacted by the fan sediments. Topographic control is also consistent with the fact that the southern part of this sub-basin, where the fan represents a topographic high, was less exposed to mass-transport deposition.

The structural control results from the weight of the Amazon deep-sea fan itself. The flexure caused by the fan load has greatly impacted the basin subsidence since the Late Miocene - Pliocene (Watts *et al.*, 2009). Here the distance between MTDs A and B is only ~10km. Nevertheless, we suggest that the presence of faults only in MTD A and not in MTD B may be related to the increased deformation near the upper domain of the fan compared to other places in equivalently proximal regions, which are all subject to basin-scale extensional constraints. This hypothesis is supported by the position of the seismic cube at the junction of three domains (shelf, fan and basin) and within a strongly flexured zone (Watts *et al.*, 2009, see Figure_Supplementary 2 in supplementary material). Moreover, the processes that might have impacted the basinward-evolving headscarps upslope, may involve partly this fan control, and partly the larger-scale gravity-tectonic deformation of the entire basin.

Finally, the Amazon River sediment discharge has kept increasing since its onset as a transcontinental river (Gorini *et al.*, 2014). This element is recovered by the basinward evolution of upslope headscarps (see section 4.6).

### 5.2. How do our new unexpected results compare with previous literature on the Amazon region?

According to our results, MTDs A and B were affected by deformation in the bottom of their head parts. Outside the MTDs, the deformed facies otherwise characterizes slope-deformed facies. Deformation within the heads of the MTDs is caused by either specific flow behavior or by post-deposition deformation or evaporite/mud-related deformation in the zone, which highlights the deposition process: MTDs onlapping the continental slope and subject to internal, very small-scale post-depositional gravity-induced deformation – or to syn-depositional viscous 'attachment' (see Moscardelli & Wood, 2008 for 'attached mass transport complexes', whose upper part shows a deformed, slump character). In 2D-based studies, scale / resolution effects may prevent 2D data from revealing such detailed variation in deformation. Note that the scale argument also tends to exclude

the impact of deformation by any tectonic- or non-tectonic process, which, given the small size of our MTDs, would probably rather affect the whole geobodies.

We have shown that our MTDs originate from upslope paleo-scarps. Former studies on the Amazon Basin revealed MTDs whose headscarps are even more distally located than the area covered by our cube. These larger, more distal MTDs have been interpreted as originating from the submarine slope (Reis *et al.*, 2016). The relationship between these two sets of MTDs has not yet been established. However, the north-northeast (NNE) principal direction of MTDs A and B suggests a link with the MTDs of the Amapá Upper Complex (Figure 6).

Our results suggest small-scale variations inside MTDs A and B. For example, MTD A includes regions, among which some have been homogenized since their deposit, and others have been subject to the presence of fluids, clasts, or apparent heterogeneity. Assessing the relevance of these internal variations is difficult when comparing to MTDs observed at basin-scale, for which no conclusion can be drawn at our finer scale. However, the frequent reworking of the recent sedimentary pile due to the influence of the fan or to the high sedimentary influx (Reis *et al.*, 2010, Reis *et al.*, 2016) supports these observations.

MTD A is not visible on any available 2D seismic line. MTD B can be found on one line, on which its extent is highly uncertain (Figure 9). Our results should thus be understood as concerning only parts (the head parts) of potentially larger MTDs (although probably not as large as the basin-scale ones).

Global analysis of the five MTDs in our cube suggested a signature of eustatic cycles in the vertical regularity of “MTD layering”, as long as this regularity is also visible in the interbedded sediments – which was not the case, making this suggestion highly uncertain. These “MTD layers” do not have the same properties (number of objects, degree of internal heterogeneity, direct above- and below-environment), so that ‘cycles’ are difficult to depict. Moreover, the average thickness of MTDs decreases from the deepest to the shallowest, i.e. it decreases with time. This is not in line with the above-mentioned increase in sediment discharge from the Amazon River; what is more, the increase is not recovered in the regular spacing between the three “MTD layers” indicated in Figure 4. Thus, no conclusion can be drawn on this potential eustatic influence. The limited content of the relation map is not yet sufficient to explain this decreasing thickness trend.

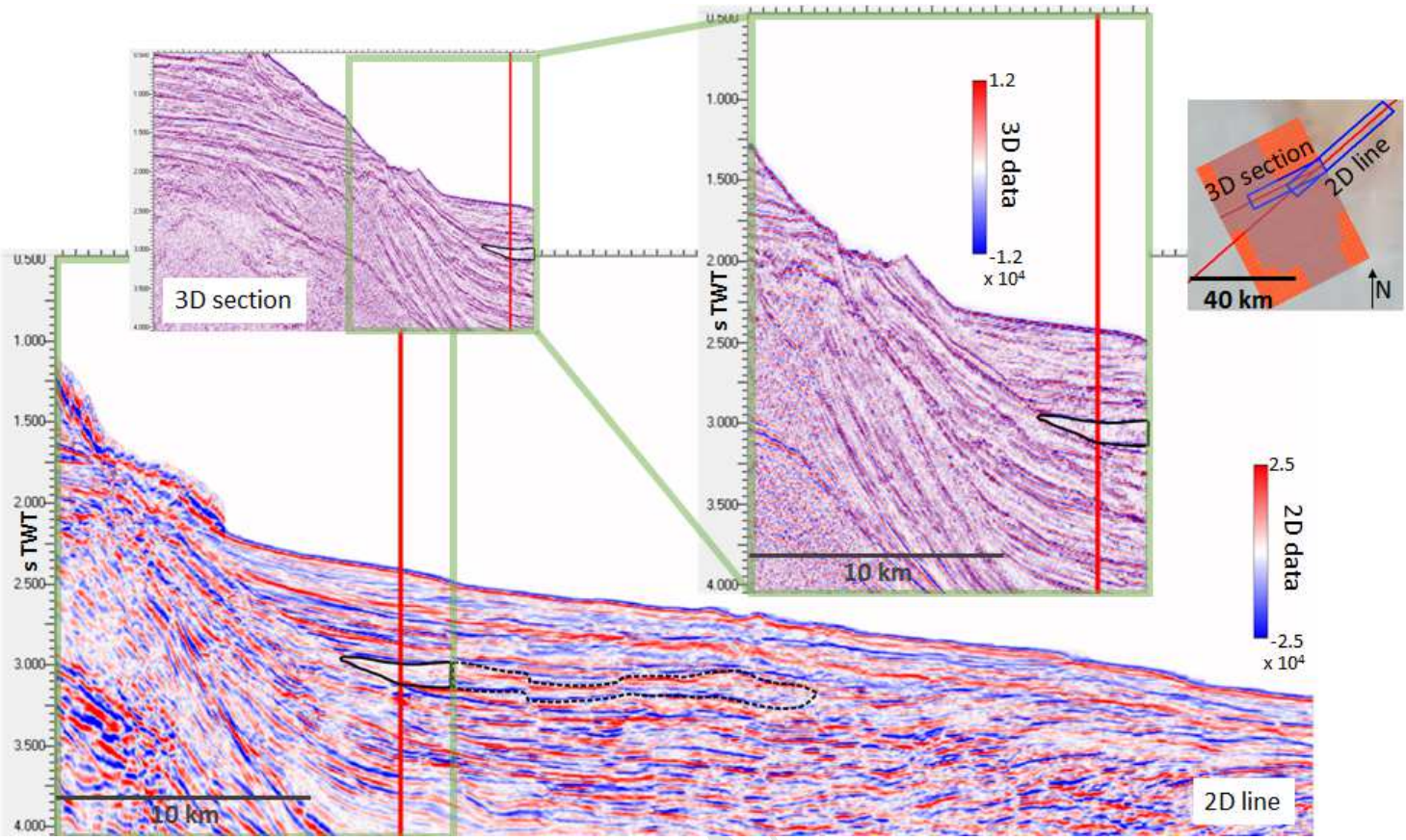


*Figure 9. MTD B illustrated on a 2D seismic line. Solid black line: contour of MTD B drawn on a section extracted from the 3D cube (projected onto the 2D line). Dashed line: possible continuation of MTD B, interpreted from the 2D data.*

Considering sections 5.1 in which our results agree with the general context of the region, and 5.2, in which most of unexpected results refer to the scale or availability of data, we propose to validate our new methodology. In section 6, we discuss its main limits and potential outlooks.

ACCEPTED MANUSCRIPT

# 6. Discussion

## 6.1. Sensitivity analysis

In the graph analyses, some processes are inferred only once from a descriptor; if the descriptor is not available, the process will not be hypothesized at all. Conversely, other processes are suggested by several different descriptors, which reduces their uncertainty. Lastly, some processes are suggested by some descriptors but contradicted by others. In this case, the hypothesis is rejected and the process is not inferred. All these analyses may differ if insufficient data content / quality prevents reliable property descriptions. Here, we assess the loss of results from our methodology for situations with deficient data, leading to one or several missing descriptors.

(i) Let us first consider the case where the thickness/resolution ratio is less than 3 (see Table_Supplementary 2). This could happen for occurrences of thin MTDs in a poorly-resolved seismic dataset. This typically limits the acquisition of Internal Facies Distribution descriptors to studies on rather shallow MTDs. If these descriptors were lacking in our application, this would reduce our confidence in several processes: the heterogeneous fluid migrations, the south-north difference of flow behavior within the MTDs and their direction change. It would also suppress hypotheses concerning preserved clasts and the different compaction/drainage processes inside the objects. Thus, this situation removes information on rather fine-scale transport properties and post-depositional processes, which may be crucial, for example, in the context of exploration.

(ii) In another case, the picking grid of surfaces (basal and upper surfaces of the MTD, headscarp) may be too low to obtain descriptors depicting the surfaces' morphologies: ramps or ridges, median slope values, presence of specific indicators like plunging pool / terracing and erosional descriptors on the basal surface. In our application, such a loss reduces our confidence in the proposed direction change (absence of the asymmetric erosive walls and of the US dip change in MTD B), and in the relatively 'fluid' behavior of the MTDs; it also cancels the hypothesis concerning post-depositional regional deformation (faults). In our case, then, only a few hypotheses would be less supported, and the post-depositional deformation could be easily guessed from global observation of the seismic data. In other cases however, the absence of 'basal ramps' and 'multi-terracing downslope' may prevent the retrieval of the 'cascading events' hypothesis for example, which could lead to mis-interpretations.

(iii) Another possible situation is that the seismic amplitude range is not appropriate or sufficiently reliable to distinguish between 'strong' and 'normal' reflectors (due to acquisition or processing uncertainties), in which case, part of the internal facies descriptors may be lacking ('transparent facies distribution', 'presence of preserved blocks') as well as the 'basal surface strong amplitude' descriptor. In our application, fluid migrations, different compaction/drainage, as well as differences in lithologies, would not be proposed at all. This supports the general need for good-quality amplitudes to assess the presence of fluid.

(iv) Finally, data coverage may limit the acquisition of several descriptors, particularly within the Morphology, Position and Global Environment properties, and also including the Headscarp descriptors and toe-related descriptors if these regions are outside the dataset. From our application, a few hypotheses would then be missing: a potential link between MTDs A and B, arguments concerning remobilization from A to B, and impact of large-scale deformations or sea-level cycles on the sedimentation in the zone. Such descriptors therefore yield crucial information on the basin- or regional-scale controls, as well as potential genetic relationships between MTDs, that may make it possible to classify them in series, or as signatures of regional events (e.g. attached MTDs). Conversely, in our study, having access to the toe region of the MTDs would have provided more indications on the paleo-seafloor topography and existing geomorphology at the time of the mass movement, as well as the flow behavior; it would also have enabled more reliable comparisons of volume and all morphological properties, yielding more constraints on the transport processes and more reliable comparisons between objects.

It is unusual that all the above mentioned data deficiencies occur simultaneously. Generally, to be identified in seismic data, an MTD has a sufficient thickness to define its basal and upper surfaces. Large MTDs are often not completely imaged by 3D seismic data with relatively good resolution, leading to either missing head or toe region; they may otherwise be studied using 2D seismic data with lower resolution but including the entire extent of the object.

Missing parts of the object will generally hide information on regional processes, whereas an entirely-imaged MTD in a poorly-resolved dataset will hide information on finer-scale transport style, posterior internal modifications and on the current state of the MTD. Too-loose picking of MTD-related surfaces leads to missing transport erosional properties and hence critical information on the flow direction and on the state of the paleo-seafloor, as well as posterior impacts of fluid migrations or large-scale deformations. However, depending on the application, interpreters use data that correspond to their needs. For reservoir-scale studies, high-resolution seismic data are preferred, while for assessing large-scale controls, datasets with larger coverage may be chosen at the expense of a lower resolution. Studies implying fluids will require precise surface definitions and a high degree

of confidence in the distribution of the seismic amplitudes. Thus, despite the lower confidence with fewer available descriptors, the graph-based methodology can also be used in applications with limited data.

### 6.2. What is the uncertainty related to our methodology?

The limited amount of data and limited information in the relation map reveal that the results produced by our methodology are subject to three main kinds of uncertainty.

The first kind of uncertainty is related to the input data. The seismic acquisition and processing stages, the interpretation of surfaces, the resolution and the coverage of the dataset are the key elements introducing uncertainty in the inputs (see preceding section). Like in any seismic interpretation, depth-converted data might also add some uncertainty, e.g. velocity pull-up/push-down effects that affect both surface and global descriptors. Additionally, the facies classification (Internal Facies descriptors) itself involves some uncertainty, although the labels given to groups of 'transparent facies', 'chaotic facies', etc., are normally checked on several seismic sections; two different geological facies may produce the same response in terms of seismic facies (e.g. Sun *et al.* (2017) show disrupted, low-amplitude patterns due to gas chimneys that might be considered 'deformed' or 'chaotic' facies). However, the descriptors used here are supported by seismic interpreters' experience. It should also be noted that initially flat morphologies and surfaces may be bent or steepened by large-scale deformation processes; this could be included in the graph (e.g. by adding an edge between nodes 'post-deposition regional deformation' and 'BS median slope') if other parts of the graph are adapted accordingly (e.g. analyzing facies distributions and surface properties along a dipping direction). For now such considerations are not included, which might limit the graph to cases with little, or known, steepening of this kind.

A second kind of uncertainty is related to the relationships, or laws, comprised in the relation map. These laws come from the literature, but they also have limits; a possible, quantitative way to take these limits into account would be to weight every edge of the graph, thereby weighting the confidence of each possible interpreted physical process during the interpretation procedure.

The final kind of uncertainty is related to the construction of the relation map. The contents of the two lists in Table 1 and Table 2 were chosen based on a bibliographical study, which is the source of two main biases:

- The number of published studies, and the number of studies we used, are limited, which necessarily limits the physical processes and MTD descriptors encountered in our study. However, we used a variety of sources, to ensure the studies came from several different

backgrounds (numerical, conceptual or analog modeling / seismic interpretation) and are as little as possible affected by this bias.

- Depending on what can be modelled and what cannot, the literature itself is biased. For example, among the links between Table 2 and Table 1, there is no direct link between trigger type and final MTD properties, because the physics that describe a trigger differ from the physics that describe a fall/flow, and to date, no study has tackled this link.

The selection of the most relevant elements to build our two lists was an iterative process. A few properties that are described in the literature were intentionally not included in this study; in particular, fine-scale properties of a wasted material, e.g. its grain size distribution or grains friction coefficients. Such properties certainly impact the mass movement, and possibly the MTD itself (e.g. when a front of larger grains generates 'tongues' at the toe of the MTD, as suggested in Pouliquen *et al.*, 1997). Yet we considered them as 'side' effects compared to others, especially since in several, the internal lithology of the MTD must be known, which is not the case in our seismic analysis. Too large-scale, or too rare, processes, such as the displacement of water that creates a propagating sea wave and may trigger other instabilities in another region of the basin, were also disregarded in our analyses. Finally, it should be noted that all the elements listed in Table 2 depend on a timescale; they should always be considered as long- or short-term *relative* to some other phenomenon.

In order to quantitatively assess this last kind of uncertainty, ideally the relation map should be further developed, to include all the relationships left out of this work, until an entire formal ontology has been created with quantitative confidence weighting on edges according to how often they are cited and/or demonstrated in the literature. This would be the ideal solution, probably very complex to reach.

This possibly high uncertainty (depending on the three factors mentioned above) is in line with the present approach of suggesting several scenarios, one of which will finally be chosen by the interpreter using other sources of information (geological context, other kinds of data such as log data that noticeably increases confidence in facies interpretations). Our approach does not make it possible to select one scenario with certainty, but rather offers several possibilities. It is an attempt to reveal an on-going interpretation procedure when only a few input data and published results are available. The interpreter then uses the results of the relation map as he/she needs them, and consequently remains the sole decision-maker.

### 6.3. Future outlook, other developments and uses of our methodology.

The graph constitutes a knowledge base using only information from the literature. The idea behind it is to convey the scientifically accepted information that already exists (within the existing nodes and edges), to be used jointly with specific information concerning a case study for applications. Improvements to the results may come from both sides (graph content and data quality). Improvements to the methodology will come from the use of the graph itself.

The first possible extension is obviously its automation through a dedicated numerical representation: the GraphML language, as promoted by e.g. Schauberger *et al.* (2016), and the Web Ontology Language (OWL)[3], as promoted by Malik *et al.* (2010) and implemented for ontology edition by Musen (2015). Many details are provided in the present paper on the steps of interpretation, descriptor by descriptor, node by node; but in a numerical framework, these results could be obtained automatically, which would considerably accelerate the process. With this view, using quantitative weights on edges, as suggested above, would certainly benefit the procedure itself, and would yield some quantitative uncertainty information. Automated acquisition of the MTD descriptors may be hard to implement, but this point can be solved separately and does not jeopardize the graph-based method itself.

Our work can be further extrapolated by using the relation map in a different way thanks to its automated (i.e. rapid) version. An interesting application would be to test several hypotheses on unknown values of certain MTD descriptors. The resulting hypothetical interpretations, if different, could be compared with outside knowledge about the MTD, thus enabling selection of the most-likely value of the descriptors of interest. Trials could then be run to see whether, based on a partial MTD characterization (i.e. having only part of MTD descriptors' values), using the relation map would make it possible to infer the values of the others. Another approach would be to input some "a-priori bias" on the edges' weights, based on external information. The results of the modified-graph would then take this information (e.g. contextual knowledge) into account.

[3] Developed by the W3 Consortium on Semantic Web: https://www.w3.org/OWL/ , last accessed Sept. 2018

# 7. Conclusion

We propose the use of an ontology for MTD interpretation in seismic data based on the combination of literature sources. To this end, we built a knowledge base from existing literature in the form of a graph (relation map). A graph-based methodology is provided to infer potential causal processes for the seismic signatures of MTDs. This novel method was applied on a case study with a 3D seismic dataset from the Amazon Basin, which validated the methodology.

Our methodology yields objective proposals for interpretation based only on the ontology and the input data, with no other prior information. Some uncertainties linked to the relation map itself and to the input data remain. In a more complete interpretation process, additional information may make it possible to select the most-likely interpretation among those proposed by our method.

Improvements in the relation map will enable quantification of the probability of each interpretation proposed. Our work is a first step towards a more complete ontology, which we believe will help share new knowledge for various uses of MTD interpretation.

# 8. Acknowledgements

We thank the CGG Houston office for data provision and permission to publish. We also thank the Brazilian National Agency of Petroleum (ANP) for data made available to A. Tadeu dos Reis (UERJ-Brazil), who is collaborating on the present research theme and on the study of the Offshore Amazon Basin. We are very grateful to: Alberto Cruz from the ISTeP laboratory (Sorbonne Université) for fruitful discussions and improvements on some of the contents of this article; Noalwenn Dubos-Sallée, from *IFP Energies Nouvelles*, for proof reading the article; and Alexandre Lethiers, from the ISTeP laboratory, for his support with the map figures. Many thanks to Tiago M. Alves and two anonymous reviewers whose comments and suggestions helped us significantly improve the content of this article.

# 9. Supplementary material

Here we give the full list of edges of the knowledge-based graph (relation map) (Table_Supplementary 1). The reference column provides non-exhaustive examples of previous studies whose results support the corresponding edges. Studies by Lafuerza *et al.* (2009), Lacoste *et al.* (2012), Frey-Martínez *et al.* (2011), Goujon *et al.* (2007), Chemenda *et al.* (2009), Elverhoi *et al.* (2010), Laberg *et al.* (2017), Li *et al.* (2017), Ogiesoba & Hammes (2012), and the Geological Survey of

Norway website (https://www.ngu.no, last accessed in January, 2018) were also used as contributions to our knowledge base, although they are not mentioned in the text of this article.

*Table_Supplementary 1. Edges of the graph. Columns indicate the source node and target node, the directed/undirected character of the edge, and reference(s) that support its definition. The second tab in the table gives all the references used in the first tab. The third tab gives all the edges connected to MTD descriptors nodes.*

***(Attached in a separate file.)***

Table_Supplementary 2 provides details on the limits of detection for the MTD descriptors listed in Table 1.

*Table_Supplementary 2. Detection limit for descriptors of Table 1, in terms of dataset coverage, resolution, and other aspects.*

***(Attached in a separate file.)***

We also provide a figure illustrating one possible visualization of the graph (Figure_Supplementary 1 (a)) and the adjacency matrix of the graph (Figure_Supplementary 1 (b)). The visualization highlights the variation in 'degree' between nodes (represented by the size of the node), indicating which nodes have the highest number of connecting nodes. The adjacency matrix shows the links between nodes directly in a less graphical way; with this matrix, we show that no direct impact has yet been proven in the literature between trigger processes and MTD descriptors. These representations were obtained using the Gephi software (https://gephi.org/).

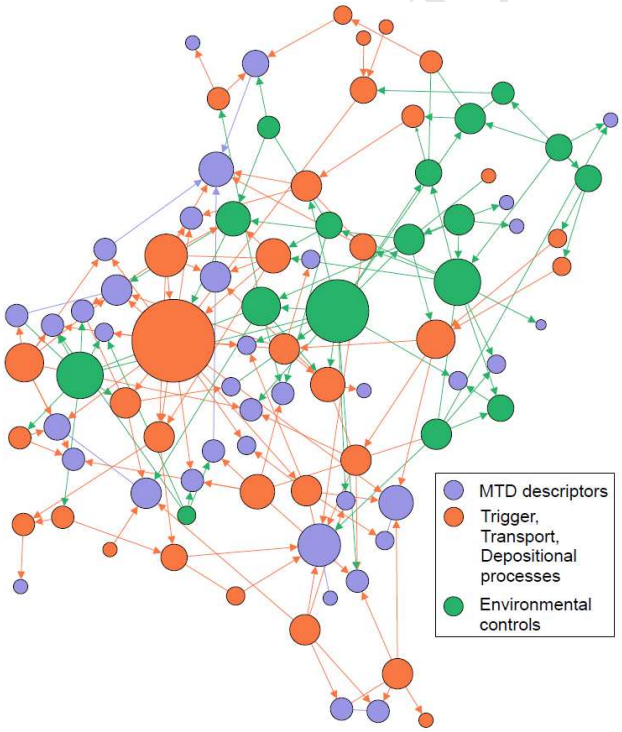


(a)

*Figure_Supplementary 1. Knowledge-based graph representations: (a) one possible visualization, and (b) adjacency matrix. Figures obtained using the Gephi software (https://gephi.org/).*

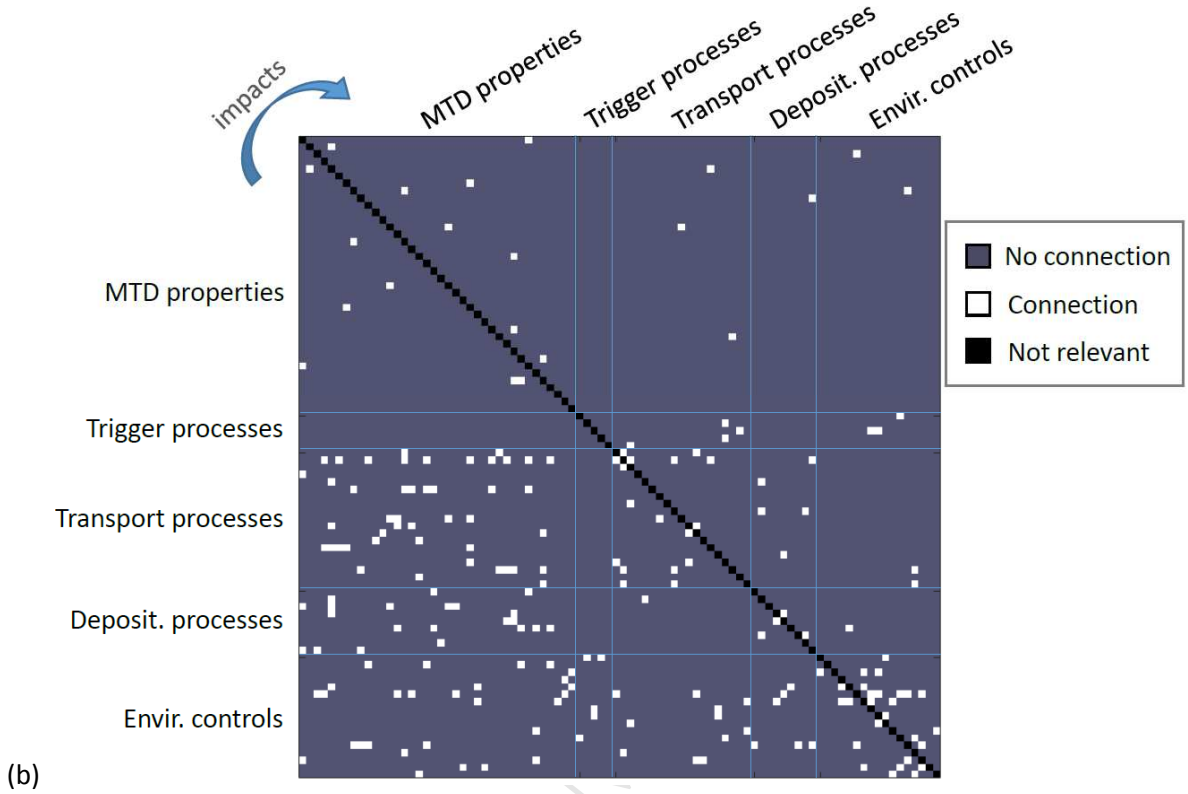


*(Figure_Supplementary 1 - continued)*

985

ACCEPTED MANUSCRIPT

Finally, we include a bathymetric map by Watts et al., 2009 (Figure_Supplementary 2), showing results of their calculation of flexure due to the fan load. The position of the seismic cube used in the present study has been added, to demonstrate its critical position and potential variations in fan-induced flexure inside the cube.

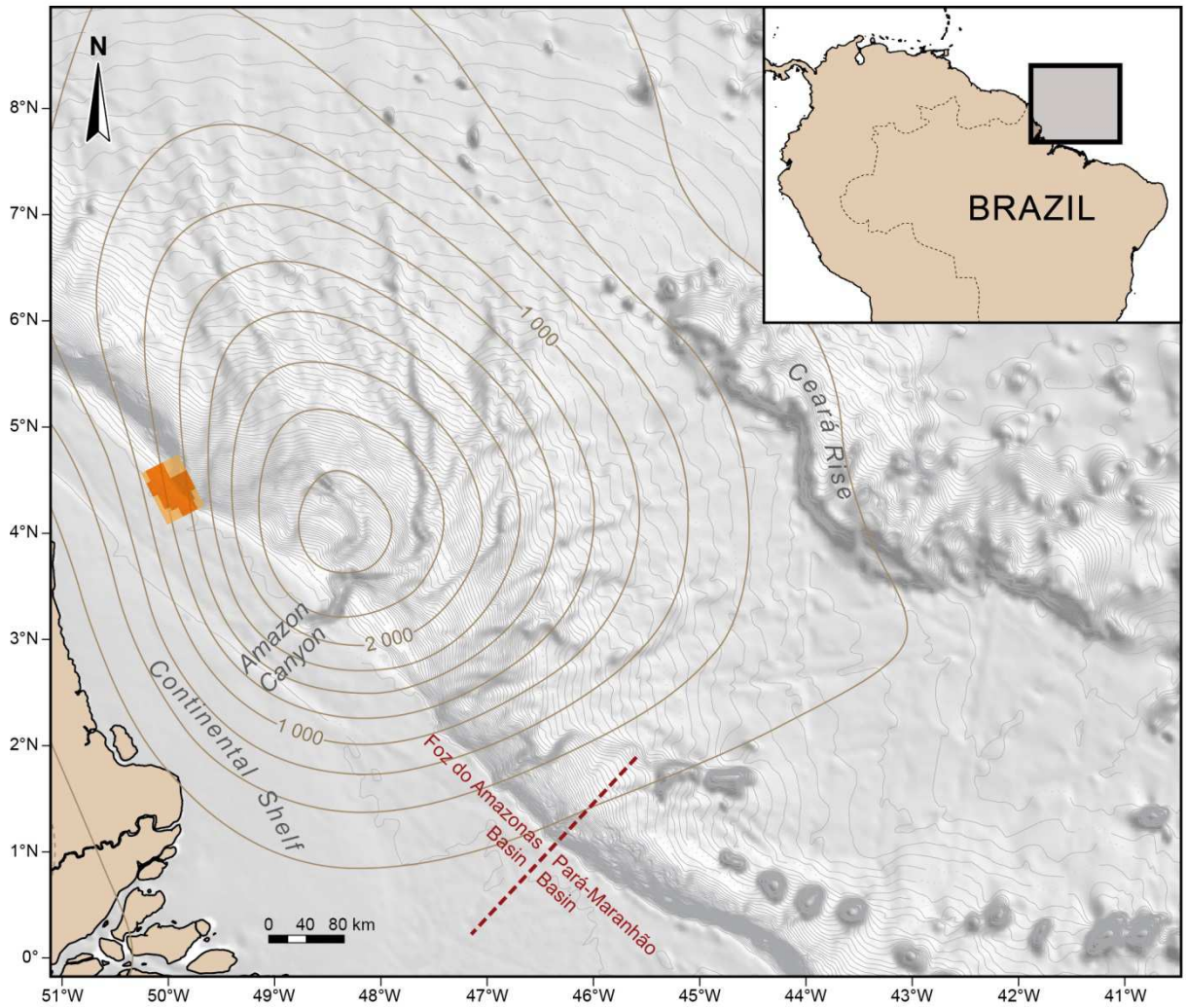


*Figure_Supplementary 2. Bathymetric map of the Offshore Amazon Basin showing the impact of flexure caused by the fan load; from Watts et al., 2009 and Rodger, 2009. Solid lines show the flexural depression (contour interval: 250 m). The inland flexural bulge is not visible on this map. The 3D seismic cube is mapped with available seismic data in dark orange.*

# References


ALVES, T.M. (2015) Submarine slide blocks and associated soft-sediment deformation in deep-water basins: A review. *Marine and Petroleum Geology*, **67**, 262–285. doi:10.1016/j.marpetgeo.2015.05.010

ALVES, T.M., KURTEV, K., MOORE, G.F. & STRASSER, M. (2014) Assessing the internal character, reservoir potential, and seal competence of mass-transport deposits using seismic texture: A geophysical and petrophysical approach. *Bulletin*, **98** (4), 793–824. doi:10.1306/09121313117

ARAÚJO, É.F.D.S., SILVA, C.G., REIS, A.T.D., PEROVANO, R., GORINI, C., VENDEVILLE, B.C. & ALBUQUERQUE, N.C.D. (2009) Movimentos de massa multiescala na bacia da foz do Amazonas - margem equatorial brasileira. *Rev. Bras. Geof.*, **27** (3), 485–508. doi:10.1590/S0102-261X2009000300013

BONDY, J.A. & MURTY, U.S.R. (2008) *Graph theory*. Springer, New York.

BOURGET, J., ZARAGOSI, S., ELLOUZ-ZIMERMANN, N., MOUCHOT, N., GARLAN, T., SCHNEIDER, J.-L., LANFUMEY, V. & LALLEMANT, S. (2011) Turbidite system architecture and sedimentary processes along topographically complex slopes: The Makran convergent margin. *Sedimentology*, **58** (2), 376–406. doi:10.1111/j.1365-3091.2010.01168.x

BULL, S., CARTWRIGHT, J. & HUUSE, M. (2009) A review of kinematic indicators from mass-transport complexes using 3D seismic data. *Marine and Petroleum Geology*, **26** (7), 1132–1151. doi:10.1016/j.marpetgeo.2008.09.011

CHEMENDA, A., BOIS, T., BOUISSOU, S. & TRIC, E. (2009) Numerical modelling of the gravity-induced destabilization of a slope: The example of the La Clapière landslide, southern France. *Geomorphology*, **109**, 86–93. doi:10.1016/j.geomorph.2009.02.025

CLARK, I.R. & CARTWRIGHT, J.A. (2009) Interactions between submarine channel systems and deformation in deepwater fold belts: Examples from the Levant Basin, Eastern Mediterranean sea. *Marine and Petroleum Geology*, **26** (8), 1465–1482. doi:10.1016/j.marpetgeo.2009.05.004

DALLA VALLE, G., GAMBERI, F., ROCCHINI, P., MINISINI, D., ERRERA, A., BAGLIONI, L. & TRINCARDI, F. (2013) 3D seismic geomorphology of mass transport complexes in a foredeep basin: Examples from the Pleistocene of the Central Adriatic Basin (Mediterranean Sea). *Sedimentary Geology*, **294**, 127–141. doi:10.1016/j.sedgeo.2013.05.012

DAMUTH, J. & EMBLEY, R. (1981) Mass-transport processes on Amazon Cone: western equatorial Atlantic. *American Association of Petroleum Geologists Bulletin*, **65** (4), 629–643.

DAMUTH, J., FLOOD, R.D., KOWSMANN, R.O., BELDERSON, R.H. & GORINI, M.A. (1988) Anatomy and growth pattern of Amazon deep-sea fan as revealed by long-range side-scan sonar (GLORIA) and high-resolution seismic studies. *AAPG Bulletin*, **72** (8), 885–911.

ELVERHOI, A., BREIEN, H., BLASIO, F.V. de, HARBITZ, C.B. & PAGLIARDI, M. (2010) Submarine landslides and the importance of the initial sediment composition for run-out length and final deposit. *Ocean Dynamics*, **60** (4), 1027–1046.

FIGUEIREDO, J., HOORN, C., VAN DER VEN, P. & SOARES, E. (2009) Late Miocene onset of the Amazon River and the Amazon deep-sea fan: Evidence from the Foz do Amazonas Basin. *Geology*, **37** (7), 619–622. doi:10.1130/G25567A.1

FREY-MARTÍNEZ, J. (2010) 3D Seismic Interpretation of Mass Transport Deposits: Implications for Basin Analysis and Geohazard Evaluation. In: *Submarine Mass Movements and Their Consequences* (Ed. by D.C. Mosher, R.C. Shipp, L. Moscardelli, J.D. Chaytor, C.D.P. Baxter, H.J. Lee & R. Urgeles), pp. 553–568. Springer Netherlands, Dordrecht.

FREY-MARTÍNEZ, J., BERTONI, C., GÉRARD, J. & MATÍAS, H. (2011) Processes of Submarine Slope Failure and Fluid Migration on the Ebro Continental Margin: Implications for Offshore Exploration and

Development. In: *Mass-Transport Deposits in Deepwater Settings* (Ed. by R.C. Shipp, P. Weimer & H.W. Posamentier), pp. 181–198. SEPM (Society for Sedimentary Geology).

GORINI, C., HAQ, B.U., DOS REIS, ANTONIO TADEU, SILVA, C.G., CRUZ, A., SOARES, E. & GRANGEON, D. (2014) Late Neogene sequence stratigraphic evolution of the Foz do Amazonas Basin, Brazil. *Terra Nova*, **26** (3), 179–185. doi:10.1111/ter.12083

GOUJON, C., DALLOZ-DUBRUJEAUD, B. & THOMAS, N. (2007) Bidisperse Granular Flow on Inclined Rough Planes. In: *Traffic and Granular Flow'05* (Ed. by A. Schadschneider, T. Pöschel, R. Kühne, M. Schreckenberg & D.E. Wolf), pp. 147–156. Springer Berlin Heidelberg, Berlin, Heidelberg.

GRUBER, T.R. (1993) A translation approach to portable ontology specifications. *Knowledge Acquisition*, **5** (2), 199–220. doi:10.1006/knac.1993.1008

LABERG, J.S., STRASSER, M., ALVES, T.M., GAO, S., KAWAMURA, K., KOPF, A. & MOORE, G.F. (2017) Internal deformation of a muddy gravity flow and its interaction with the seafloor (site C0018 of IODP Expedition 333, Nankai Trough, SE Japan). *Landslides*, **14** (3), 849–860. doi:10.1007/s10346-016-0766-7

LACOSTE, A., VENDEVILLE, B.C., MOURGUES, R., LONCKE, L. & LEBACQ, M. (2012) Gravitational instabilities triggered by fluid overpressure and downslope incision – Insights from analytical and analogue modelling. *Journal of Structural Geology*, **42**, 151–162. doi:10.1016/j.jsg.2012.05.011

LAFUERZA, S., SULTAN, N., CANALS, M., FRIGOLA, J., BERNÉ, S., JOUET, G., GALAVAZI, M. & SIERRO, F.J. (2009) Overpressure within upper continental slope sediments from CPTU data, Gulf of Lion, NW Mediterranean Sea. *Int J Earth Sci (Geol Rundsch)*, **98** (4), 751–768. doi:10.1007/s00531-008-0376-2

LEE, H.J., LOCAT, J., DESGAGNS, P., PARSONS, J.D., MCADOO, B.G., ORANGE, D.L., PUIG, P., WONG, F.L., DARTNELL, P. & BOULANGER, E. (2007) Submarine Mass Movements on Continental Margins. In: *Continental Margin Sedimentation* (Ed. by C.A. Nittrouer, J.A. Austin, M.E. Field, J.H. Kravitz, J.P.M. Syvitski & P.L. Wiberg), pp. 213–274. Blackwell Publishing Ltd, Oxford, UK.

LEE, S.E., TALLING, P.J., ERNST, G.G. & HOGG, A.J. (2002) Occurrence and origin of submarine plunge pools at the base of the US continental slope. *Marine Geology*, **185** (3-4), 363–377. doi:10.1016/S0025-3227(01)00298-5

LEYNAUD, D., MIENERT, J. & VANNESTE, M. (2009) Submarine mass movements on glaciated and non-glaciated European continental margins: A review of triggering mechanisms and preconditions to failure. *Marine and Petroleum Geology*, **26** (5), 618–632. doi:10.1016/j.marpetgeo.2008.02.008

LI, W., ALVES, T.M., URLAUB, M., GEORGIOPOULOU, A., KLAUCKE, I., WYNN, R.B., GROSS, F., MEYER, M., REPSCHLÄGER, J., BERNDT, C. & KRASTEL, S. (2017) Morphology, age and sediment dynamics of the upper headwall of the Sahara Slide Complex, Northwest Africa: Evidence for a large Late Holocene failure. *Marine Geology*, **393**, 109–123. doi:10.1016/j.margeo.2016.11.013

MALIK, Z., REZGUI, A., MEDJAHED, B., OUZZANI, M. & KRISHNA SINHA, A. (2010) Semantic integration in Geosciences. *Int. J. Semantic Computing*, **04** (03), 301–330. doi:10.1142/S1793351X10001036

MANGENEY-CASTELNAU, A., BOUCHUT, F., VILOTTE, J.P., LAJEUNESSE, E., AUBERTIN, A. & PIRULLI, M. (2005) On the use of Saint Venant equations to simulate the spreading of a granular mass. *J. Geophys. Res.*, **110** (B9). doi:10.1029/2004JB003161

MARFURT, K.J. & ALVES, T.M. (2015) Pitfalls and limitations in seismic attribute interpretation of tectonic features. *Interpretation*, **3** (1), SB5-SB15. doi:10.1190/INT-2014-0122.1

MASLIN, M., VILELA, C., MIKKELSEN, N. & GROOTES, P. (2005) Causes of catastrophic sediment failures of the Amazon Fan. *Quaternary Science Reviews*, **24** (20-21), 2180–2193. doi:10.1016/j.quascirev.2005.01.016

MERRIS, R. (2001) *Graph theory*. Wiley, New York [u.a.].

MIENERT, J. (2009) Methane Hydrate and Submarine Slides. In: *Encyclopedia of Ocean Sciences*, pp. 790–798. Elsevier.

MOSCARDELLI, L. & WOOD, L. (2008) New classification system for mass transport complexes in offshore Trinidad. *Basin Research*, **20** (1), 73–98. doi:10.1111/j.1365-2117.2007.00340.x

MOURGUES, R. & COBBOLD, P.R. (2006) Sandbox experiments on gravitational spreading and gliding in the presence of fluid overpressures. *Journal of Structural Geology*, **28** (5), 887–901. doi:10.1016/j.jsg.2005.12.013

MOURGUES, R., LACOSTE, A. & GARIBALDI, C. (2014) The Coulomb critical taper theory applied to gravitational instabilities. *J. Geophys. Res. Solid Earth*, **119** (1), 754–765. doi:10.1002/2013JB010359

MOURGUES, R., LECOMTE, E., VENDEVILLE, B. & RAILLARD, S. (2009) An experimental investigation of gravity-driven shale tectonics in progradational delta. *Tectonophysics*, **474** (3-4), 643–656. doi:10.1016/j.tecto.2009.05.003

MULDER, T. & ALEXANDER, J. (2001a) Abrupt change in slope causes variation in the deposit thickness of concentrated particle-driven density currents. *Marine Geology*, **175** (1-4), 221–235. doi:10.1016/S0025-3227(01)00114-1

MULDER, T. & ALEXANDER, J. (2001b) The physical character of subaqueous sedimentary density flows and their deposits. *Sedimentology*, **48** (2), 269–299. doi:10.1046/j.1365-3091.2001.00360.x

MUSEN, M.A. (2015) The Protégé Project: A Look Back and a Look Forward. *AI matters*, **1** (4), 4–12. doi:10.1145/2757001.2757003

NELSON, C.H., ESCUTIA, C., DAMUTH, J.E. & TWICHELL, D.C. (2011) Interplay of Mass-Transport and Turbidite-System Deposits in Different Active Tectonic and Passive Continental Margin Settings: External and Local Controlling Factors. In: *Mass-transport deposits in deepwater settings* (Ed. by R.C. Shipp, P. Weimer & H.W. Posamentier), pp. 39–66. SEPM (Society for Sedimentary Geology), Tulsa (Okla.).

OGIESOBA, O. & HAMMES, U. (2012) Seismic interpretation of mass-transport deposits within the upper Oligocene Frio Formation, south Texas Gulf Coast. *Bulletin*, **96** (5), 845–868. doi:10.1306/09191110205

OMOSANYA, K.O. & ALVES, T.M. (2013) Ramps and flats of mass-transport deposits (MTDs) as markers of seafloor strain on the flanks of rising diapirs (Espírito Santo Basin, SE Brazil). *Marine Geology*, **340**, 82–97. doi:10.1016/j.margeo.2013.04.013

ORTIZ-KARPF, A., HODGSON, D.M., JACKSON, C.A.-L. & MCCAFFREY, W.D. (2016) Mass-transport complexes as markers of deep-water fold-and-thrust belt evolution: Insights from the southern Magdalena fan, offshore Colombia. *Basin Res*, **57** (4), 294. doi:10.1111/bre.12208

OWEN, M., DAY, S. & MASLIN, M. (2007) Late Pleistocene submarine mass movements: Occurrence and causes. *Quaternary Science Reviews*, **26** (7-8), 958–978. doi:10.1016/j.quascirev.2006.12.011

POSAMENTIER, H.W. & MARTINSEN, O.J. (2011) The Character and Genesis of Submarine Mass-Transport Deposits: Insights from Outcrop and 3D Seismic Data. In: *Mass-transport deposits in deepwater settings* (Ed. by R.C. Shipp, P. Weimer & H.W. Posamentier), pp. 7–38. SEPM (Society for Sedimentary Geology), Tulsa (Okla.).

POULIQUEN, O., DELOUR, J. & SAVAGE, S.B. (1997) Fingering in granular flows. *Nature*, **386** (6627), 816–817. doi:10.1038/386816a0

REIS, A.T., ARAUJO, E., SILVA, C.G., CRUZ, A.M., GORINI, C., DROZ, L., MIGEON, S., PEROVANO, R., KING, I. & BACHE, F. (2016) Effects of a regional décollement level for gravity tectonics on late Neogene-

Quaternary large-scale slope instabilities in the Foz do Amazonas Basin, Brazil. *Marine and Petroleum Geology*, **75**, 29–52.

REIS, A.T., PEROVANO, R., SILVA, C.G., VENDEVILLE, B.C., ARAUJO, E., GORINI, C. & OLIVEIRA, V. (2010) Two-scale gravitational collapse in the Amazon Fan: A coupled system of gravity tectonics and mass-transport processes. *Journal of the Geological Society*, **167** (3), 593–604. doi:10.1144/0016-76492009-035

REITSMA, F., LAXTON, J., BALLARD, S., KUHN, W. & ABDELMOTY, A. (2009) Semantics, ontologies and eScience for the geosciences. *Computers & Geosciences*, **35** (4), 706–709. doi:10.1016/j.cageo.2008.03.014

RICHARDSON, S.E.J., DAVIES, R.J., ALLEN, M.B. & GRANT, S.F. (2011) Structure and evolution of mass transport deposits in the South Caspian Basin, Azerbaijan. *Basin Research*, **23** (6), 702–719. doi:10.1111/j.1365-2117.2011.00508.x

RODGER, M. (2009) *A marine geophysical study of the Amazon continental margin, North-Eastern Brazil*. University of Oxford, Oxford, UK.

ROY, A., ROMERO-PELÁEZ, A.S., KWIATKOWSKI, T.J. & MARFURT, K.J. (2014) Generative topographic mapping for seismic facies estimation of a carbonate wash, Veracruz Basin, southern Mexico. *Interpretation*, **2** (1), SA31-SA47. doi:10.1190/INT-2013-0077.1

SAWYER, D.E., FLEMINGS, P.B., BUTTLES, J. & MOHRIG, D. (2012) Mudflow transport behavior and deposit morphology: Role of shear stress to yield strength ratio in subaqueous experiments. *Marine Geology*, **307-310**, 28–39. doi:10.1016/j.margeo.2012.01.009

SCHAUBERGER, B., ROLINSKI, S. & MÜLLER, C. (2016) A network-based approach for semi-quantitative knowledge mining and its application to yield variability. *Environ. Res. Lett.*, **11** (12), 123001. doi:10.1088/1748-9326/11/12/123001

SHIPP, R.C., WEIMER, P. & POSAMENTIER, H.W. (2011) Mass-Transport Deposits in Deepwater Settings: An Introduction. In: *Mass-transport deposits in deepwater settings* (Ed. by R.C. Shipp, P. Weimer & H.W. Posamentier), pp. 3–6. SEPM (Society for Sedimentary Geology), Tulsa (Okla.).

SILVA, C.C., DOS REIS, A.T., PEROVANO, R.J., GORINI, M.A., DOS SANTOS, M.V.M., JECK, I.K., TAVARES, A.A.A. & GORINI, C. (2016) Multiple Megaslide Complexes and Their Significance for the Miocene Stratigraphic Evolution of the Offshore Amazon Basin. In: *Submarine Mass Movements and their Consequences* (Ed. by G. Lamarche, J. Mountjoy, S. Bull, T. Hubble, S. Krastel, E. Lane, A. Micallef, L. Moscardelli, C. Mueller, I. Pecher & S. Woelz), pp. 49–60. Springer International Publishing, Cham.

SILVA, C.G., ARAÚJO, E., REIS, A.T., PEROVANO, R., GORINI, C., VENDEVILLE, B.C. & ALBUQUERQUE, N. (2010) Megaslides in the Foz do Amazonas Basin, Brazilian Equatorial Margin. In: *Submarine Mass Movements and Their Consequences* (Ed. by D.C. Mosher, R.C. Shipp, L. Moscardelli, J.D. Chaytor, C.D.P. Baxter, H.J. Lee & R. Urgeles), pp. 581–591. Springer Netherlands, Dordrecht.

SUN, Q., ALVES, T., XIE, X., HE, J., LI, W. & NI, X. (2017) Free gas accumulations in basal shear zones of mass-transport deposits (Pearl River Mouth Basin, South China Sea): An important geohazard on continental slope basins. *Marine and Petroleum Geology*, **81**, 17–32. doi:10.1016/j.marpetgeo.2016.12.029

SUTTON, J.P. & MITCHUM, R.M. (2011) Upper Quaternary Seafloor Mass-Transport Deposits at the Base of Slope, Offshore Niger Delta, Deepwater Nigeria. In: *Mass-Transport Deposits in Deepwater Settings* (Ed. by R.C. Shipp, P. Weimer & H.W. Posamentier), pp. 85–110. SEPM (Society for Sedimentary Geology).

TALLING, P.J., MASSON, D.G., SUMNER, E.J. & MAGESINI, G. (2012) Subaqueous sediment density flows: Depositional processes and deposit types. *Sedimentology*, **59** (7), 1937–2003. doi:10.1111/j.1365-3091.2012.01353.x

URGELES, R. & CAMERLENGHI, A. (2013) Submarine landslides of the Mediterranean Sea: Trigger mechanisms, dynamics, and frequency-magnitude distribution. *J. Geophys. Res. Earth Surf.*, **118** (4), 2600–2618. doi:10.1002/2013JF002720

URLAUB, M., TALLING, P.J. & MASSON, D.G. (2013) Timing and frequency of large submarine landslides: Implications for understanding triggers and future geohazard. *Quaternary Science Reviews*, **72**, 63–82. doi:10.1016/j.quascirev.2013.04.020

VANNESTE, M., SULTAN, N., GARZIGLIA, S., FORSBERG, C.F. & L'HEUREUX, J.-S. (2014) Seafloor instabilities and sediment deformation processes: The need for integrated, multi-disciplinary investigations. *Marine Geology*, **352**, 183–214. doi:10.1016/j.margeo.2014.01.005

VARNES, D.J. (1958) Landslide Types and Processes. *Landslides and engineering practice*, **24**, 20–47.

VERNEY, P. (2009) *Interprétation géologique de données sismiques par une méthode supervisée basée sur la vision cognitive*, Informatique. Ecole Nationale Supérieure des Mines de Paris, Paris.

WANG, C., MA, X. & CHEN, J. (2018) Ontology-driven data integration and visualization for exploring regional geologic time and paleontological information. *Computers & Geosciences*, **115**, 12–19. doi:10.1016/j.cageo.2018.03.004

WATTS, A.B., RODGER, M., PEIRCE, C., GREENROYD, C.J. & HOBBS, R.W. (2009) Seismic structure, gravity anomalies, and flexure of the Amazon continental margin, NE Brazil. *J. Geophys. Res.*, **114** (B7), 17. doi:10.1029/2008JB006259

WOODHOUSE, M.J., THORNTON, A.R., JOHNSON, C.G., KOKELAAR, B.P. & GRAY, J.M. T. (2012) Segregation-induced fingering instabilities in granular free-surface flows. *J. Fluid Mech.*, **709**, 543–580. doi:10.1017/jfm.2012.348

WU, S.-G., QIN, Z.-L., WANG, D.-W., PENG, X.-C., WANG, Z.-J. & YAO, G.-S. (2011) Analysis on Seismic Characteristics and Triggering Mechanisms of Mass Transport Deposits on the Northern Slope of the South China Sea. *Chinese J. Geophys.*, **54** (6), 1056–1068. doi:10.1002/cjg2.1684

ACCEPTED MANUSCRIPT

# List of Figures and Tables

Figure 1. (a) Schematic representation of our graph (relation map). Dots are nodes, colored according to their category (environmental controls, mass movement (MM) properties or mass transport deposit (MTD) descriptors); lines/arrows are undirected/directed edges. Interpretation of MTD descriptor 2 yields nodes C and E as direct potential impacting processes, then nodes A and B; node 3 is only related to node 2. (b) Representation of a sub-part of the global knowledge base, with nodes mentioned in the proposed application (section 4). ..... 8

Figure 2. Bathymetric map of the Offshore Amazon Basin with the location of major previously-studied MTDs and seismic data used in this article. Modified from Reis et al., 2016 and Silva et al., 2016. The 50°W (Damuth & Embley, 1981), WMTD, EMTD (Western / Eastern MTDs, Damuth et al., 1988) are superficial MTDs. URMTD and BMTD (Unit R / Buried MTDs, Damuth et al., 1988) are buried. The Amapá and Pará-Maranhão Megaslides (ALC-AUC / PMM) were studied by Silva et al., 2010 and Reis et al., 2016. Amapá Lower Complex (ALC), the deepest mass transport complex of Amapá, is mapped in blue; Amapá Upper Complex (AUC), more recent, is mapped in orange, after Reis et al., 2016. The 3D seismic cube is mapped with available seismic data in dark orange and 2D seismic profiles are mapped in dark red. ..... 18

Figure 3. 3D view of the five MTDs highlighted in the studied data. MTDs D and E are separated by the brown dashed line. Colored surfaces are upslope scarps. Grey sections are seismic sections from the seismic cube. The largest blue surface is the top of the carbonate platform (see also Gorini et al., 2014)..... 21

Figure 4. The 5 MTDs highlighted in one seismic section of the post-stack seismic cube (uninterpreted and interpreted seismic sections). MTDs A and B appear to mark the beginning of seismic unit II above seismic unit I. The 3 stratigraphic periods for MTD deposition are separated by roughly similar thicknesses. ..... 22

Figure 5. Precise meaning ascribed to each facies used in this study, coupled with examples on seismic sections (shown as green patches on top of the seismic sections). Facies were interpreted based on an automatic method developed by the IFPEN research group, not detailed in this paper. 23

Figure 6. MTDs A and B slope maps of basal surfaces (BS) and upper surfaces (US). Dip direction shown by color hue, dip value by brightness. Both MTDs show a lateral erosive wall in their BS southern regions, and a change in BS and US dip orientation, indicating a change in orientation of the flow. Faults are visible on the BS and US of MTD A. Interpreted map shows a strong amplitude 'corridor' and two topographic depressions of the BS, retrieved from amplitude and topographic maps respectively. Amapá Upper Complex is described by Reis et al. 2016 (see Figure 2). ..... 26

Figure 7. MTD A (dashed circle). Seismic section (a) and seismic facies (b). Faults and topographic depression are highlighted, with possible plowing (sensu Posamentier & Martinsen, 2011) on the high-amplitude negative-polarity basal surface (BS) of MTD A. Irregular high amplitudes are also visible inside MTD A. Deformed facies rather appears at the head part of MTD A (similar distribution for C). ..... 29

Figure 8. Upslope scarps showing fore-stepping evolution of the erosion on one dip seismic section from our seismic cube. ..... 31

Figure 9. MTD B illustrated on a 2D seismic line. Solid black line: contour of MTD B drawn on a section extracted from the 3D cube (projected onto the 2D line). Dashed line: possible continuation of MTD B, interpreted from the 2D data..... 38

Figure_Supplementary 1. Knowledge-based graph representations: (a) one possible visualization, and (b) adjacency matrix. Figures obtained using the Gephi software (https://gephi.org/)..... 46
Figure_Supplementary 2. Bathymetric map of the Offshore Amazon Basin showing the impact of flexure caused by the fan load; from Watts et al., 2009 and Rodger, 2009. Solid lines show the flexural depression (contour interval: 250 m). The inland flexural bulge is not visible on this map. The 3D seismic cube is mapped with available seismic data in dark orange..... 47

Table 1. Characteristic properties of MTDs and their descriptors. BS: Basal Surface, US: Upper Surface, HS: Headscarp. ..... 10
Table 2. Environmental controls and mass movement properties. 'Mass movement properties' comprise properties of the trigger phase, the transport phase and the deposition phase (possibly including post-deposition modifications). 'Environmental controls' are large-scale processes..... 12

Table_Supplementary 1. Edges of the graph. Columns indicate the source node and target node, the directed/undirected character of the edge, and reference(s) that support its definition. The second tab in the table gives all the references used in the first tab. The third tab gives all the edges connected to MTD descriptors nodes. ..... 45
Table_Supplementary 2. Detection limit for descriptors of Table 1, in terms of dataset coverage, resolution, and other aspects..... 45

## Sizes (desired width) and colors of Figures and Tables

Figure 1. 2 columns if (a) and (b) are stacked horizontally, 1 column otherwise. Color needed.
Figure 2. 1.5 columns. Color needed.
Figure 3. 2 columns. Color needed.
Figure 4. 1.5 columns. Color needed.
Figure 5. 2 columns. Color needed.
Figure 6. 1.5 to 2 columns. Color needed.
Figure 7. 1 column (or 2 columns, (a) and (b) stacked horizontally). Color needed.
Figure 8. 2 columns. Color needed.
Figure 9. 2 columns. Color needed.
Table 1. 2 columns. No need for color.
Table 2. 2 columns. No need for color.

Table_Supplementary 1, Table_Supplementary 2, Figure_Supplementary 1 and Figure_Supplementary 2 are supplementary material.

ACCEPTED MANUSCRIPT

ACCEPTED MANUSCRIPT

| Descriptors | Properties |
|---|---|
| thickness variation | **Morphology** |
| average thickness | |
| width variation | |
| horizontal aspect ratio | |
| volume | |
| surface area | |
| maximum horizontal length | |
| principal direction | |
| presence of 'tongues' at toe | |
| BS median slope | **Basal surface** |
| BS flat sub-horizontal zone | |
| plunging pool indicator | |
| multiple terracing downslope | |
| BS ramps | |
| scours, grooves or striations | |
| lateral erosive walls | |
| BS strong amplitude | |
| US median slope | **Upper surface** |
| US ramps or ridges | |
| US with turbidites on top | |
| upward connection to other MTDs | **Position** |
| lateral connection to other MTDs | |
| near structural elements laterally | |
| runout distance | |
| HS downslope evolution | **Headscarp** |
| HS morphology | |
| presence of preserved blocks | **Internal facies distributions** |
| preserved blocks size | |
| chaotic facies distribution | |
| transparent facies distribution | |
| faulty facies distribution | |
| ridged facies distribution | |
| thrust fault angle increase to toe | |
| lithology distribution in MTD | |
| deformed facies distribution | |
| MTD proportion in sedimentary pile | **Global environment** |
| lateral distribution of MTDs | |
| vertical distribution of MTDs | |

ACCEPTED MANUSCRIPT

ACCEPTED MANUSCRIPT

gravity, short term
seismicity, short term
fluid overpressure, short term
offshore events and waves
chemical effects
flow velocity and energy
flow behavior: elastic, plastic, fluid
local fluidization
local thickening of flowing material
volume of transported material
flow direction
modifying basin morphology
inducing seismicity
triggering turbidity current
triggering cascading mass movements
erosion of underlying material
plunging pool effect
plowing effect on underlying material
detached MTD
grains heterogeneity in flowing mass
fluid overpressure on basal surface
fluid overpressure in moving mass
initial potential energy of mass
lithology in transported mass
frontal compression
loss of mass
remobilization
compaction during burial
posterior fluid migrations
post deposition regional deformation
trigger turbidity current at stop
post deposition of turbidites
terminal dispersion
seismicity or waves, long term
evaporite deformation & mud volcanism
sea level evolution
basin depocenter position
subsidence/uplift, extension/compression
existing geomorphology, objects and pathways
sedimentation rate and type
pore pressure increase by compression
pore pressure increase by fluid migration
permeability increase
lithology of underlying material in source zone
initial aspect ratio and top of mass slope angle
topography confinement downwards
seafloor effective friction angle
seafloor shapes and dip variations
source domain in basin
lithology of underlying material downslope

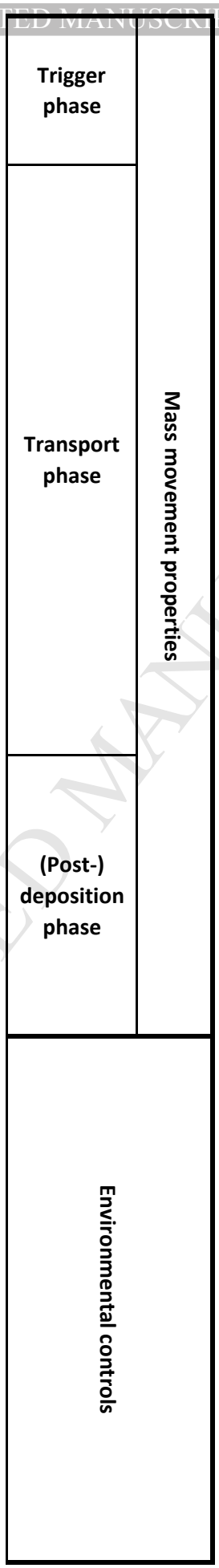


ACCEPTED MANUSCRIPT